INTERACTIONS BETWEEN CONFINED CALCITE SURFACES IN AQUEOUS SOLUTIONS

A Surface Forces Apparatus Study

Joanna Dziadkowiec

THESIS

for the degree of

Philosophiae Doctor

Faculty of Mathematics and Natural Sciences

Department of Physics

University of Oslo, Norway

October 2018

ACKNOWLEDGEMENTS

This project has received funding from the European Union's Horizon 2020 research and innovation programme NanoHeal under the Marie Skłodowska-Curie grant agreement No 642976. My thanks go to the whole NanoHeal Team: it was a great experience to be a part of the NanoHeal network and learn about geology, physics, chemistry, materials, and calcite together. Thank you for sharing your knowledge and for a great company when travelling together. Special thanks to Magdalena for her help in coordinating this project, to Dag for starting this network, to Bahareh and Agnes Piednoir for helping me during my secondment in Université Claude Bernard Lyon 1, and to Martin Mosquet and LafargeHolcim company for explaining everything about concrete to me.

I want to thank my supervisor Anja Røyne for a prompt introduction to the project; for showing me that it can be easy to work with the Surface Forces Apparatus; for making sure that I will make the best use of all my experimental results; and for always having time for discussions. I am happy to have been learning from you for the last three years. I also want to thank my co-supervisor, Dag Kristian Dysthe, for always challenging my understanding of how the things work and for sharing his knowledge. My thanks go to all members of the PGP-NJORD group. It was great to spend this time among you, chat, discuss, learn from your experience, and get inspired when listening about your research. Special thanks to Shaka with whom I spend plenty of time doing experiments in the lab. It was great to solve many calcite puzzles together.

Many thanks to Jon Einar Bratvold and Ola Nilsen for enthusiastically preparing multiple calcite samples that I used in this project. I also want to acknowledge Berit Løken Berg and Siri Simonsen for the help with SEM and Ole Bjørn Karlsen for his useful advice. Last but not least, I want to thank my family for always cheering me on!

CONTENTS

CHAPTER 1

INTRODUCTION

The macroscopic mechanical strength of rocks and mineral-based materials is frequently controlled by microscale and nanoscale mechanisms occurring at discrete solid-solid contacts. The interfaces between two solids are critical to deformation processes as they enable and govern mass transport within the material, confine fluids that facilitate chemical reactions, and allow the slip movement along the grain boundaries and fractures. Solid-solid contacts are also discrete regions in which adhesive or repulsive surface forces may operate. The surface forces are affected not only by the properties of the solid phases but also by the chemistry of the medium confined between the surfaces. Both surface forces and mineral reactivity can render the solid-solid interfaces stronger or weaker. Adhesive surface forces or cementing growth of minerals will strengthen the interfaces. Conversely, repulsive surface forces or displacive mineral growth will make the interfaces weaker. As the possible links between surface forces and reactivity of confined mineral surfaces are not fully explored yet, the complete understanding of all the processes that may affect the interfacial strength is lacking. In this thesis, I tackle the question of to what extent the nanoscale surface forces acting between reactive individual mineral surfaces may contribute to the macroscopic strength and cohesion of rocks and granular materials.

Calcite (calcium carbonate) is a mineral of interest since it is relatively reactive in contact with water, and it is one of the most abundant minerals in the Earth's crust. Marine organisms started precipitating calcite hundreds of millions of years ago to build their shells and skeletons. This biogenic calcite material, subjected to slow sedimentation and lithification, has later formed vast limestone and chalk rock deposits. We now use these calcite resources to build, to make paper

and plastics, to clean the air, or to prepare medicines. Whether these are shells of organisms, rocks or man-made products, calcite-based materials are usually composed of aggregates of calcite grains. It is important what keeps these grains together. Organisms use organic molecules and controlled crystallization in confined spaces. In rocks, the overburden pressure and pore fluids act together to dissolve, rearrange, cement and consolidate the calcite grains together. People adjust calcite properties using mechanical processing, high temperature, or chemical methods. In order to gain a further insight into all these processes, one can measure interactions at a level of single calcite grains. Simultaneous measurements of surface forces acting between two surfaces and surface reactivity in the Surface Forces Apparatus (SFA) provide such an opportunity.

This experimental thesis is based on the measurements of surface forces acting between two calcite surfaces using the SFA. The focus lies on how aqueous solutions of various chemical composition influence both the forces acting between two calcite surfaces and calcite reactivity. In Manuscript 1, the surface forces have been investigated in water. Electrolyte solutions of varying composition and concentrations have been used in Manuscript 2. The influence of water-soluble organic molecules with varying sizes has been investigated in Manuscript 3. Based on these experiments, I discuss what are the implications of the measured forces in relation to geological environments and calcite-based materials.

CHAPTER 2

SCIENTIFIC BACKGROUND

2.1 Calcite in geological environments

Calcium carbonate ($CaCO_3$) is a simple ionic compound that forms calcite - one of the most abundant minerals in the Earth's crust. Despite its uncomplicated chemical composition, $CaCO_3$ displays a great structural variability: it can crystallize in several polymorphic forms that differ in crystal structures and degrees of hydration. Among them, only trigonal calcite is thermodynamically stable at atmospheric temperature and pressure conditions [1]. Many factors, such as the relative ratio of dissolved Ca^{2+}/CO_3^{2-} ionic species or the presence of impurities, can promote the stability of the other $CaCO_3$ polymorphs, explaining precipitation of aragonite, vaterite and amorphous calcium carbonate (ACC) at thermodynamically unfavorable conditions. The focus of this thesis lies on the most abundant polymorph - calcite.

Most of the calcite found in geological environments was precipitated by marine organisms [2]. Accumulation and lithification of calcite (mainly of biogenic origin) in sedimentary basins started on a global scale over hundreds of millions of years ago and led to the formation of vast limestone and chalk deposits. Although these carbonate rocks are not the most abundant sediments in the upper Earth's crust, their relatively high porosity makes them important drinking water aquifers [3] and oil reservoirs (~60% of the known petroleum reserves is found in carbonates [4, 5]). Limestones, chalks and other carbonate rocks such as dolomites (composed of $CaMg(CO_3)_2$) are also crucial as climate-regulating rocks since they serve as a long time CO_2 storage. The ongoing acidification of oceans, due to the increasing content of CO_2 dissolved in

water, is affecting the stability and precipitation of the modern carbonate sediments [6]. **Figure 1** illustrates how the increasing partial pressure of CO_2 enhances the solubility of calcite, and thus of the carbonate rocks.

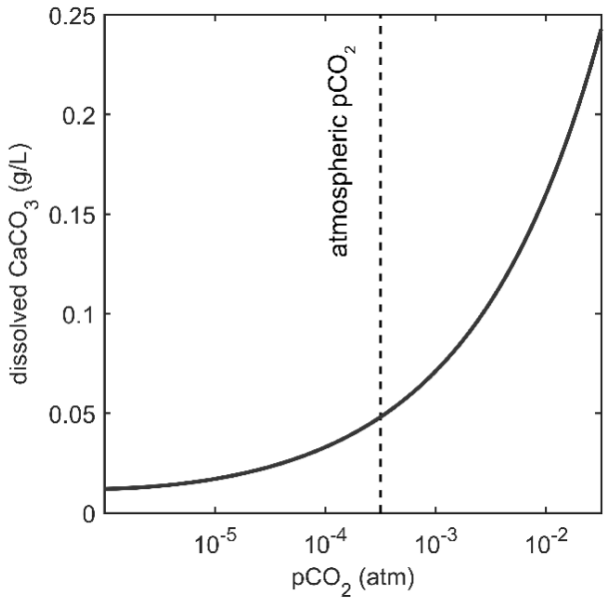

***Figure 1**. Increasing solubility of calcite with the increasing partial pressure of CO_2 (pCO_2) calculated in the PhreeqC [7] software.*

Despite the high sensitivity of calcite to varying levels of dissolved CO_2, its solubility is relatively low in comparison with other common ionic minerals. The solubility of calcite in water is over 10 000 times lower than the solubility of NaCl at the same temperature and pressure conditions. On the other hand, calcite solubility generally exceeds the solubilities of various aluminosilicate minerals that prevail in sedimentary rocks. Calcite undergoes more dissolution in contact with meteoric waters (which are slightly acidic due to dissolved CO_2) than aluminosilicates. This is manifested by spectacular cavity-rich karst topographies exposed on the surface and below the ground in many places around the world (**Figure 2**). In the subsurface, the overburden pressure acts to reduce the porosity of rocks. Also there, the percolating fluids still distinctively affect the reactivity of carbonate rocks, which is reflected in their pronounced chemical compaction [4].

Compaction, which is the process of porosity reduction in sedimentary rocks, generally occurs by two distinct mechanisms: mechanical or chemical compaction. Whereas mechanical compaction involves processes such as grain rearrangement, pore collapse and brittle fracturing of grains or intracrystalline plasticity, chemical compaction occurs by fluid-assisted grain

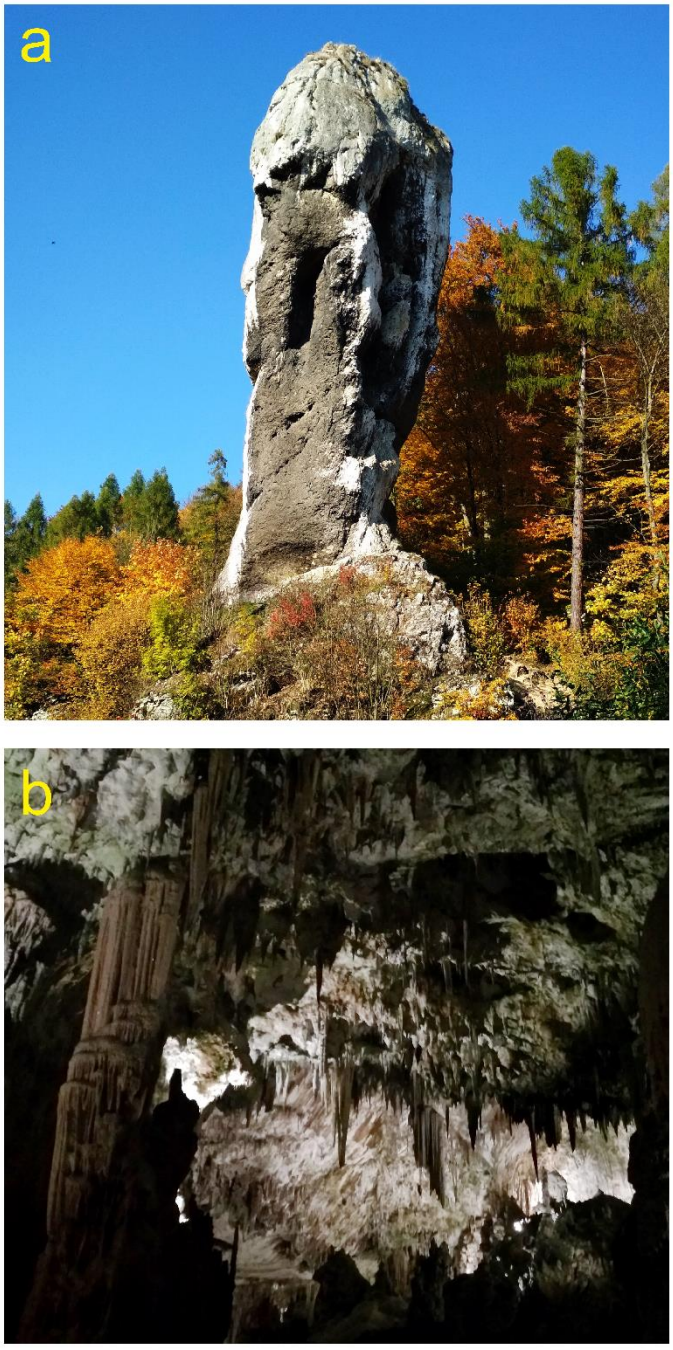

Figure 2. *Examples of karst in limestones: a) 25 meters-high isolated rock composed of the resistant skeletal Jurassic limestone* in *Ojców, Poland; b) Postojna cave created by the Pivka river in Cretaceous limestone, Slovenia.*

alteration [8, 9]. In siliceous sediments, mechanical compaction processes dominate up to 2-3 km in the subsurface, and chemical compaction becomes dominant only at greater depths [10]. There is no such strong distinction between these two mechanisms in carbonate rocks: It is acknowledged that lithification of carbonates is strongly influenced by fluid-driven chemical compaction processes already at relatively shallow depths of several hundred meters [4]. Porosity reduction can additionally occur through cementation [11]. However, the cementation process may in some cases contribute to porosity preservation by creating a stress-resistant network of cemented grains [12]. The experimental studies on the deformation of carbonates show a large variation in strain rates, depending on the sample structure [8, 9, 13-19]. Such differences in mechanical properties can be explained by the great textural variability of carbonates, which is related to both their biogenic origin and to the characteristics of their depositional environments [5]. In contrast to other sedimentary rocks, carbonates accumulate *in situ*, with little transport and material sorting. Thus, the typically observed carbonate lithofacies can be often correlated with the biofacies, characteristic for a given carbonate-forming organism [2].

The diversity of carbonate rocks complicates the systematic understanding of the rate-determining processes of carbonate deformation [4]. Regardless of that, there is a large interest to be able to understand and predict the macroscopic mechanical behavior of carbonates. Carbonate rocks are dominant hydrocarbon reservoirs and potential underground storage sites of CO_2 [20]. The accelerated deformation of carbonate reservoirs triggered by anthropogenic fluid extraction and injection operations may extensively affect rock permeability and the regional fluid flow [21]. Recent examples from carbonate oil fields indicate that a rapid exchange of reservoir-saturating fluids and reservoir depletion may induce substantial on-site reservoir compaction, which often causes flooding and infrastructure damage [22]. Moreover, active faults hosted in carbonate rocks are often responsible for upper crust-seismicity [23]. The microstructural evolution of carbonate rocks due to pressure-enhanced dissolution and reprecipitation may contribute to the sealing of active faults [24-27].

2.2 Chemical compaction of carbonates

Pressure solution

Fluid-assisted chemical compaction of carbonates is of the major interest to this thesis. Chemical compaction of sedimentary rocks encompasses plastic and brittle deformation processes that are activated in the presence of reactive fluids and stress, such as: dissolution, precipitation, mineral phase conversion, or subcritical crack propagation [4, 8, 28, 29]. The thorough examination of the microstructures of compacted carbonates found both in natural

settings [21, 30] and in the experimentally deformed samples [16, 31] leaves no doubt that pressure solution is one of the key mechanisms in the chemical compaction of carbonates. Pressure solution is a slow [32], ductile deformation and involves three main processes: 1) dissolution of contacting mineral grains along the stressed grain boundary; 2) diffusion of the dissolved species to pore spaces where the solute concentration is lower; and 3) precipitation of material on the less stressed crystal faces or further transport by diffusion and advection [33-35]. Stylolites (**Figure 3**), clay seams, sutured grain contacts, indented grains and cemented microcracks are the most typical pressure solution microstructures [4, 36, 37].

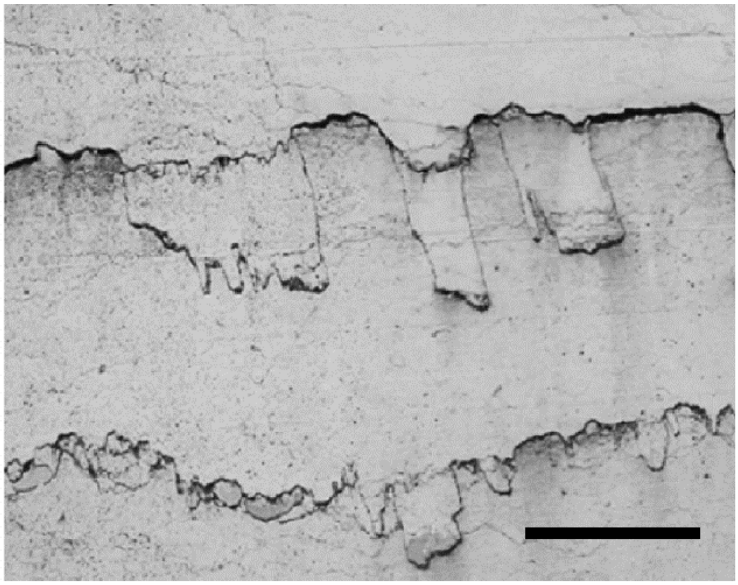

Figure 3. *Stylolites developed in a limestone rock (Burgundy, France). Scale bar is 1 cm. Photo courtesy of Francois Renard.*

Pressure solution is initiated by changes in the solid's chemical potential along a stressed mineral interface. If a flat, loaded mineral face is in equlibrium with its saturated solution, dissolution can occur only if there is an increase in normal stress (σ_n), which drives a change in the solid's chemical potential (μ):

$$\mu = f^s + \sigma_n/\rho_s \qquad \textit{(Eq. 1)}$$

where f^s is the specific Helmholtz free energy of the solid with density ρ_s [38]. If dissolution progresses, then the fluid in contact with the dissolving solid becomes supersaturated and precipitation will occur on the less stressed solid faces. For such material redistribution to occur,

the liquid film separating the two surfaces must be preserved, which means that the pressure in this film must be higher than the pressure of the bulk fluid [33, 34, 39].

The pressure in the liquid film confined between two solid surfaces is referred to as disjoining pressure and it can be understood as a difference in pressure of a film between two surfaces and the hydrostatic pressure of the bulk fluid. Disjoining pressure (Π) depends on the film thickness (x), which is reflected in the following definition:

$$\Pi = -\frac{1}{A}\frac{\partial G}{\partial x}|_{A,T,P} \qquad (Eq.\ 2)$$

where ∂G is the change in Gibbs energy with distance per constant unit area A, at fixed temperature (T) and external pressure (P) conditions [40]. If the disjoining pressure of a confined water film is positive, it is larger than the fluid hydrostatic pressure and work has to be performed to displace the water from the gap between the surfaces. Negative disjoining pressure means that the fluid film is unstable, and it migrates into the bulk solution. Positive and negative disjoining pressures corresponds respectively to repulsive and attractive surface forces. It has been experimentally measured that for smooth mineral surfaces, the disjoining pressure can be of a significant magnitude at separations below several nm [41-44].

The stability of a liquid film confined between two surfaces can be also expressed in terms of interfacial energies. Interfacial energy is a change in free energy when the interface separating two immiscible phases is expanded by one unit area [45]. Thus, the energy change of separating two similar surfaces 1 in liquid medium 3 (W_{131}) can be defined as:

$$W_{131} = 2\gamma_{13} - \gamma_{11} \qquad (Eq.\ 3)$$

where γ_{13} is solid-liquid and γ_{11} is solid-solid interfacial energy expressed per unit area, assuming smooth surfaces and no energy dissipation [45], as shown in **Figure 4.**

If $W_{131} < 0$, then two liquid-solid (1-3) interfaces have the smaller energy ($2\gamma_{13}$) than the solid-solid interface (1-1; γ_{11}), and the liquid medium will spontaneously separate two 1-1 surfaces. This scenario corresponds to the positive disjoining pressure in the liquid film. As such, the properties of the surfaces and a liquid film determine if the disjoining pressure is positive or negative. γ_{11} is also equal to the free surface energy of solid 1 and represents the energy cost to increase the surface of the solid by unit area. The water-solid interfacial energies of hydrophilic minerals are generally much smaller than their surface free energies. This means that once

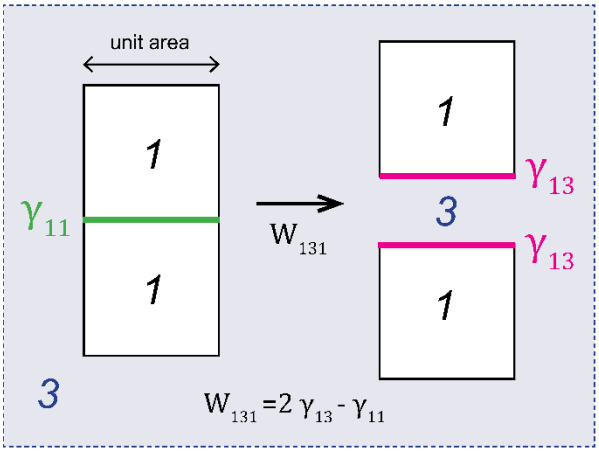

Figure 4. *Change of energy W_{131} on separating two similar surfaces 1 in a liquid medium 3. γ_{13} is solid-liquid interfacial energy and γ_{11} is solid-solid interfacial energy (= surface free energy of solid 1). Energies were expressed per unit area, assuming flat surfaces and no energy dissipation as heat or due to solid interface deformation. Modified from Israelachvili [45] (see Figure 17.1, therein).*

a crystal is cleaved or fractured in humid air, a thin layer of water will quickly adsorb on the newly exposed surfaces, making it difficult to 'heal' the fracture.

The presence of nm-thick water films is crucial in pressure solution processes, largely because such films enable transport of material by keeping the two opposing mineral surfaces separated [33, 34, 39]. Importantly, the equilibrium thickness of the confined fluid films depends not only on the applied pressure and surface energies of the confining surfaces but also on the chemical composition of the confined fluid [43, 45]. The mutual relationship of these parameters can be understood by considering surface forces.

Only a few works have investigated how surface forces contribute to the disjoining pressure in the context of pressure solution [25, 39, 46-48]. The disjoining pressure is considered to be relevant down to several km-deep regions, where it may exceed the overburden pressure [48]. Positive disjoining pressure (repulsive force) can be related to the electrostatic charge of mineral surfaces [39, 45]. It has been suggested that the thicknesses of confined liquid films can be reasonably predicted with depth, based on the surface charge of the confining, stressed mineral surfaces [39]. Mineralogy-dependent variations in the surface charge were then proposed to explain the enhanced pressure solution of quartz in the presence of mica: The surface of mica has a higher negative surface charge and can stabilize thicker water films than quartz [46]. These works have neglected the possible changes in the surface charge due to the changing fluid

composition. Other works have suggested that a varying balance of attractive and repulsive surface forces must operate at different stages of pressure solution as the magnitude and range of surface forces strongly depend on the type and concentration of ions in a confined solution [47]. Variations in surface forces with time is expected for reactive surfaces such as calcite, because calcite recrystallization affects the fluid composition. Surface forces acting across fluid films confined between surfaces will be discussed in detail in section 2.3.

For pressure solution to continue, the dissolved material must be removed from the contact region by diffusion. Otherwise, the confined solution will become saturated with respect to the stressed crystal surface and the dissolution stops. The driving force for diffusion out of the contact region is a solute concentration (φ in $mol \cdot m^{-3}$) gradient between the contact region and the bulk solution, which can be illustrated with the Fick's diffusion law in one dimension: $J = -D\frac{d\varphi}{dx}$, where J is diffusion flux (in $mol \cdot m^{-2} \cdot s^{-1}$), D is diffusion coefficient ($m^2 \cdot s^{-1}$), and x is position (m) [49]. We can thus expect that the transport of dissolved solids will depend on both the diffusion coefficient and the diffusion path, apart from the concentration gradient. The diffusion coefficient (D) in sub-nm confined water films can be lower than in bulk water, which may be understood in terms of the increased viscosity (η) of the confined films: $D = \frac{kT}{6\pi\eta\delta}$, according to Stokes-Einstein equation where k is Boltzmann constant, T is temperature and δ is particle size [50]. It has been shown, however, that ionic species can enter films that are initially thinner than their hydrated diameter with diffusion coefficients similar as in the bulk water [47], and that the decreased diffusion coefficients in sub nm-thick fluid films should not significantly influence the transport in thin water films in buried mineral interfaces [51]. Thus, the diffusion in confined spaces should be generally influenced to a larger extent by tortuosity of the diffusion path and by the inhomogeneous solute concentration across the interface. These are determined by the roughness of the contact [52, 53]. Due to the high reactivity of calcite, pressure solution in carbonates is often believed to be controlled by diffusion, being the slowest rate-determining step [16, 37, 54]. Because of that, there is a need to better understand the relationship between the interface roughness and the diffusive transport across the confined solid contact. Since all pressure solution processes take place in confined spaces, cementation and crystallization processes in spatial confinement should be better explored. It has recently been shown that the precipitation of calcite between two solid surfaces can be hindered at separations as large as 1 μm, leading to the stabilization of amorphous calcium carbonate [55]. Also, precipitation of calcite in pressure solution experiments has been shown to occur in solutions initially undersaturated with respect to calcite [56]. The reactivity of calcite in confinement is discussed in section 2.6

Water-weakening

Another commonplace deformation phenomenon in carbonates is the water-weakening. Water-weakening encompasses all the processes that lead to a substantial loss of mechanical strength in fluid-saturated rocks [57], without the direct action of the overburden pressure. Water-induced deformation frequently occurs below a critical stress at which the failure of the dry rock would occur [58]. Early reports of water-weakening in rocks point to a mineralogy-dependence and a decisive contribution of processes occurring in fractures and at grain boundaries [59-61]. Observations of water-enhanced subcritical fracturing in poorly soluble materials have led to the conclusion that effects other than simple chemical dissolution must also act at solid interfaces. It was found that the decrease of solid surface free energy due to water adsorption on mineral surfaces [62] (**Figure 4**), or a preferential hydrolysis of strained mineral bonds [63] can induce the weakening.

Porous carbonate rocks such as chalk are especially prone to water weakening [64]. The seabed subsidence in the Ekofisk oil field in Norway due to the injection of low salinity water [22] has raised a great motivation to identify which is the dominant microscale compaction mechanism in chalks. In their thorough analysis of chalk deformation in the presence of water, Risnes *et al.* [57] suggested that effects such as: chalk dissolution [65], relatively slower pressure solution [18], or destruction of capillary bridges present in dry chalk [66] are not sufficient to

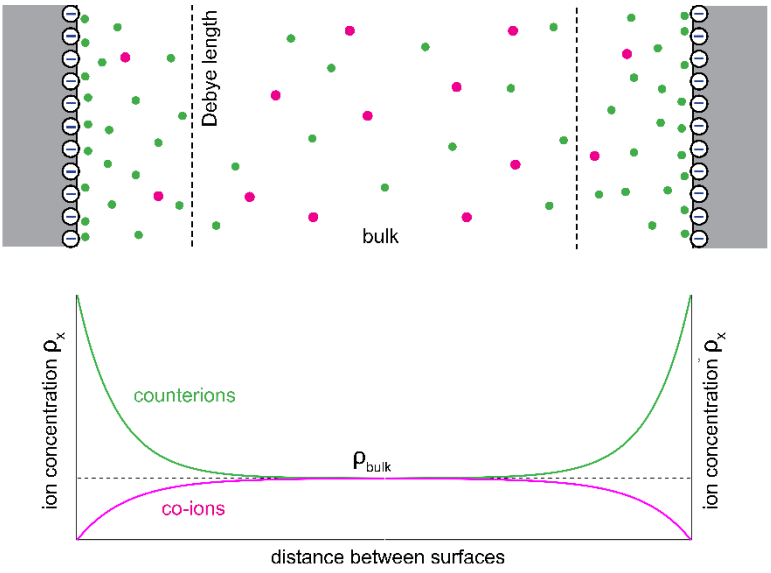

***Figure 5**. Schematic representation of ion distribution near two opposing negatively charged surfaces, showing the accumulation of cations close to the surfaces. Modified from Israelachvili, see reference [45]* and Figure 14.7 therein.

account for the observed rapid loss of the mechanical strength in water. They suggested that the deformation has been driven by the repulsive surface forces due to the adsorption of water on calcite grains, which was indicated by the observed correlation between the decreasing mechanical strength and the increasing activity of water. Later experiments by Røyne *et al.* [29, 44] have confirmed that the surface energy of calcite decreases with the increasing water activity, and that the strong repulsive surface forces operate between two calcite surfaces immersed in water.

There have been several studies in which the weakening of chalk in contact with water and fluids of varying salinity has been related to interactions between the contacting calcite grains: as the fluid salinity changes, the electrostatic forces between two calcite surfaces become more or less repulsive, due to the changes in both the calcite surface charge and the concentration of adsorbed ions [67-71]. The concentration of counterions on a mineral surface (ρ_s) depends on the mineral surface charge (σ) and can be approximated as:

$$\rho_s = \rho_0 + \frac{\sigma^2}{2\varepsilon_o \varepsilon kT} \qquad \textit{(Eq. 4)}$$

where ρ_0 is the bulk concentration, ε_o is the vacuum permittivity, ε is the water dielectric constant, k is the Boltzmann constant and T is temperature [45]. It has to be noted that σ also depends on the solution chemistry: It is a fraction of the maximum possible charge of a given surface (σ_0), and depends on the number of surface sites (α) that are charged in a given solution: $\sigma = \alpha\sigma_0$ [45]. The density of the counterions is the highest on the surface and decreases exponentially to the bulk as schematically shown in **Figure 5**. This higher concentration of ions near surfaces gives rise to electrostatic repulsion between similarly charged surfaces because when the surfaces approach each other, the regions with a higher concentration of counterions start to overlap (see section 2.3).

There is no consensus on to what extent such variations in ion distribution, which lead to the presence electrostatic forces, can explain the deformation in chalk, as it has been observed that various ionic species give rise to the varying trends in the experimentally measured deformation rates of chalk [68, 69]. In many cases, mineral dissolution and reprecipitation has been suggested to have a larger influence on the deformation processes in chalks saturated with saline solutions than possible electrostatic interactions [58, 69, 72].

How calcite grains interact with each other in natural chalk (and limestone) rocks is greatly complicated by the presence of organic material adsorbed on mineral surfaces [73]. Preserved remnants of calcite biominerals formed by organisms are commonly present in chalk (**Figure 6**),

suggesting that surface-adsorbed organic material protects them from recrystallization in water [74]. Such surfaces are heterogeneous, with randomly distributed hydrophobic and hydrophilic areas [74-76].

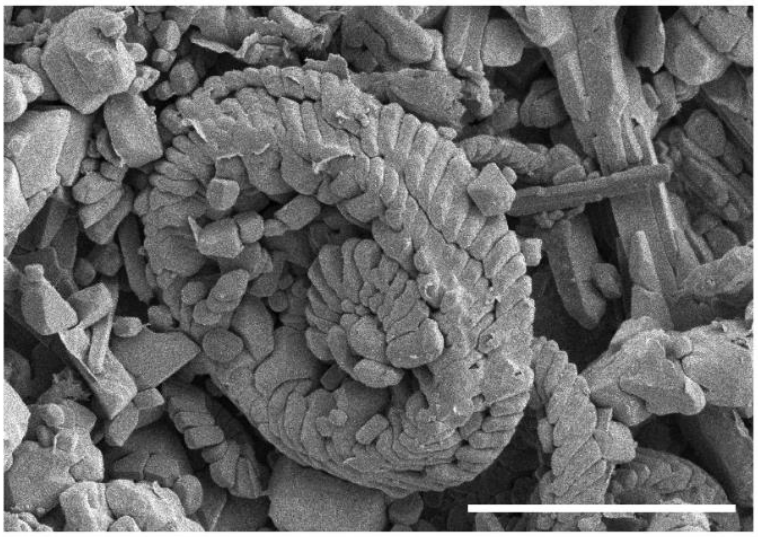

***Figure 6**. Scanning Electron Microscopy (SEM) image showing Liège chalk (Belgium) with preserved oval coccoliths plates made of biogenic calcite (formed by coccolithophores algae), and rhombohedral crystals of inorganic calcite. Scale bar is 50 μm. Image courtesy of Anne Schad Bergsaker.*

Because of a large interest in Enhanced Oil Recovery (EOR) from carbonate oil reservoirs, there is a great number of works which study how to desorb hydrocarbon molecules from calcite surfaces (e.g. [75-81]). A great number of such studies propose that the desorption can be achieved by changing the electrostatic interactions between calcite and hydrocarbon molecules from attractive to repulsive. The electrostatic forces can be modulated by adjusting the salinity of the water in contact with calcite and hydrocarbons [76]. This affects the charge of both calcite surfaces and oil molecules. Although it is expected that the desorption should be the most effective at low fluid salinity (when the repulsive electrostatic forces have the largest range), there is no agreement about the effectiveness of this mechanism. The reason for that is related to a great variability in the type of present hydrocarbon molecules (with polar and non-polar functional groups) [76, 81, 82], heterogeneity of calcite surfaces [74, 77] and ion-specific effects [80, 83, 84] that may control oil-oil, oil-calcite and calcite-calcite interactions. Due to the same effects, a full understanding of the deformation by water weakening in carbonate rocks is challenging.

2.3 Surface forces

It has been discussed in the previous section how nanometer-range surface forces may influence the deformation processes in carbonate rocks. Here, the theory related to attractive and repulsive surface forces is briefly presented. The total interaction between two charged surfaces in water can be in many cases sufficiently described by the Derjaguin– Landau – Verwey – Overbeek (DLVO) theory of colloidal stability [85, 86], which considers the joint action of attractive Van der Waals (VdW) forces and repulsive electrical double layer (EDL) forces.

Van der Waals forces

Van der Waals (VdW) forces act between all atoms and molecules. For nonpolar atoms, VdW forces are mainly related to dispersion forces which originate due to instantaneous dipole moments generated by electrons fluctuating in their positions. Instantaneous dipoles can polarize nearby atoms or molecules, leading to attractive forces acting between them [45]. As such, VdW forces always act also between macroscopic surfaces. VdW forces between two surfaces depend on the geometry of the contact. This is because they can be considered as the total interaction energy of atoms of one surface with atoms of the second surface, which are included within a given contact. VdW forces are not additive: interaction energies for each atom pair are affected by the presence of other atoms nearby.

The following expression can be used to calculate VdW forces (F_{VdW}) acting between two surfaces in crossed-cylinder geometry (which is used in the Surface Forces Apparatus experiments):

$$F_{VdW} = -\frac{AR}{6D^2} \qquad (Eq.\ 5)$$

where A is Hamaker constant, R is the radius of curvature of cylindrical samples, and D is the distance between the surfaces [45]. The VdW interaction energy (W_{VdW}) for the same geometry is:

$$W_{VdW} = -\frac{AR}{6D} \qquad (Eq.\ 6)$$

The Hamaker constant can be calculated based on the Lifshitz theory [87], using the static dielectric constants and refractive indices of interacting surfaces and of the medium across which the surfaces interact. Thus, VdW forces depend not only on the properties of the surfaces but also on the properties of the solution between the surfaces. VdW forces acting between two identical mineral surfaces across water are always attractive. The experimentally determined Hamaker constant of two interacting mica surfaces in the inert air is A_{mam} = 13.5·10^{-20} J, and it is several

times lower in water: A_{mwm} = 2.2·10^{-20} J [45]. This is generally true for all mineral surfaces. VdW forces are generally not largely affected by the salinity of water medium. A typical range of VdW forces for two calcite surfaces in water (calculated using A_{cwc} = 1.44·10^{-20} J [88]), where the forces are of significant magnitude (> 0.01 mN/m), is ~15 nm.

Electrical Double Layer forces

Although VdW forces act between mineral surfaces already at such large separations, the surfaces must be usually placed much closer to each other to experience attraction in electrolyte solutions. The reason for that is generally the presence of the electrical double layer (EDL), which is populated by an increased concentration of counterions relative to the bulk solution (as shown in **Figure 4**). Counterions accumulate near surfaces because of the surface charge. Most mineral surfaces become charged when immersed in water or an electrolyte solution. There are three main mechanisms that can cause charging of a mineral surface in the presence of an aqueous solution: 1) dissociation of protruding surface groups; 2) adsorption of ions from the solution; or 3) charge exchange between dissimilar surfaces placed in contact [45]. Some minerals, such as clays, can also have a permanent surface charge due to the metal atom substitutions (e.g. Al^{3+} for Si^{4+}) in their aluminosilicate layers [89]. If two mineral surfaces are similarly charged in an aqueous solution, they repel each other by EDL electrostatic forces.

In a simple case of a 1:1 electrolyte composed of monovalent ions (z = 1), and low surface potential of isolated surfaces (ψ_0 < 25 mV) EDL forces (F_{EDL}) can be estimated with the following linearized expression for a crossed-cylinder SFA geometry:

$$F_{EDL} = 4\pi R \varepsilon_0 \varepsilon \kappa \psi_0^2 e^{-\kappa D} \qquad (Eq.\ 7)$$

where R is the radius of the SFA cylindrical samples, ε_o is vacuum permittivity, ε is water dielectric constant, κ^{-1} is Debye length and D is separation between surfaces. The Debye length describes the width of the electric double layer, in which the concentration of counterions is larger, and can be calculated based on the solution composition:

$$\kappa = \sqrt{\sum_i \frac{C_i e^2 z_i^2}{\varepsilon_0 \varepsilon k T}}, \qquad (Eq.\ 8)$$

where C_i is bulk concentration of each ionic species i in the solution (M), k is Boltzmann constant and T is temperature. The relation between surface charge (σ) and surface potential of isolated surfaces (ψ_0) can be estimated from (for ψ_0 < 25 mV):

$$\sigma = \varepsilon_0 \varepsilon \kappa \psi_0 \quad \text{(Eq. 9)}$$

Equations 7, 8 and 9 are given in Israelachvili [45]. In the above simplified equations, it is assumed that surface potential and surface charge do not vary as the separation (D) between the surfaces changes. This is not the case, because the total number of ions in the gap between the surfaces is changing with D. Also, the number of the charged surface sites drops as the counterions are forced to adsorb onto the surface sites upon decreasing D. It is possible to obtain more correct EDL force expressions which account for these effects by solving the Poisson-Boltzmann equation [90]. However, Eq. 7 can generally be assumed to be correct at separations > 5 nm.

The magnitude and range of EDL forces depend strongly not only on the electrolyte concentration but also on the valency of the ionic species in the solution. Divalent and trivalent ions can bind to the charged surface sites more effectively in comparison with the monovalent ions and reduce σ to a larger extent. Continued adsorption of di- and trivalent ions can sometimes lead to the surface charge reversal effect, even at low bulk concentrations [45, 91].

The DLVO theory

Assuming that only VdW and EDL forces act between two mineral surfaces in an electrolyte solution, the total interaction can be described according to the DLVO theory as a sum of these two contributions:

$$F_{DLVO} = F_{VdW} + F_{EDL} \quad \text{(Eq. 10)}$$

Figure 7a illustrates how the total DLVO force between two similar mineral surfaces in 1:1 electrolyte solution varies with the changing surface charge, and **Figure 7b** shows how the DLVO force is affected by the changes in 1:1 electrolyte concentration. The EDL force component is highly sensitive to the solution composition and chemistry, whereas the VdW force is always attractive for two similar mineral surfaces and is not affected by the solution chemistry to a major extent. It can be observed that the EDL forces are the weakest for the lowest surface charge or for the highest electrolyte concentration. If the surface charge is high, there is a large repulsive EDL barrier that prevents the surfaces from adhering to each other. The area of this barrier, in the repulsive part of the force curve (force > 0), determines how much work has to be performed to bring the two surfaces into an adhesive contact. If the surface charge is relatively high and the concentration of the electrolyte is moderate, there might be a secondary minimum before

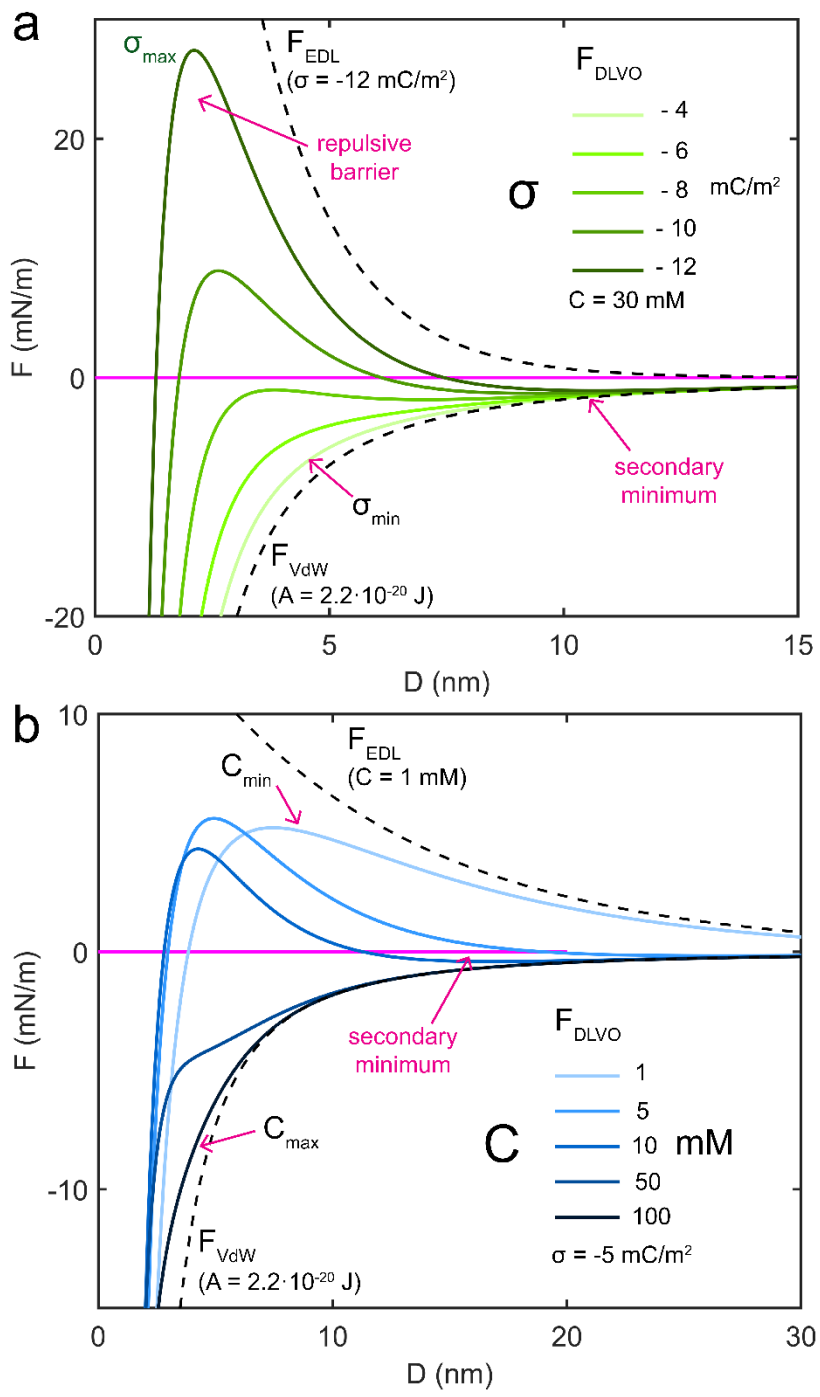

Figure 7. *DLVO forces (F) as a function surface separation (D) for varying* ***a)*** *surface charge (σ) at a fixed electrolyte concentration (C = 30 mM); and* ***b)*** *1:1 electrolyte concentration (C) at a fixed surface charge (σ = -5 mC/m²). Variations in σ due to the changing electrolyte concentration were ignored. All curves were calculated using Eq. 5, 7 and 9 and Hamaker constant A = 2.2·10⁻²⁰ J. Figure 7a has been partially modified from Israelachvili [45] (see Figure 14.13 therein).*

the strongly repulsive barrier (as indicated in **Figure 7a**). In such a secondary minimum, the attractive force is however relatively weak, and surfaces can only weakly adhere to each other.

Therefore, according to the DLVO theory, there are two main possible strategies to bring the two surfaces into an adhesive contact [40, 45, 85, 86]:

1. decreasing the surface charge (e.g. by changing pH or adding multivalent cations to the solution; **Figure 7a**);
2. increasing the electrolyte concentration in order to screen the EDL repulsion (**Figure 7b**).

Other forces

There are other interactions that can significantly affect forces between mineral surfaces such as: capillary, solvation, hydrophobic, steric, ion correlation, hydration forces, etc. [40, 45, 92]. Two last interactions: hydration forces and ion correlation forces may be especially important when considering interactions between calcite surfaces [29, 41, 93]. Hydration forces are repulsive, whereas ion correlation forces may contribute to the strong attraction between surfaces.

Hydration forces are short-range structural forces that arise due to the adsorption of water on hydrophilic mineral surfaces [92]. These forces act in the very proximity of mineral surfaces and counteract the VdW attractive forces [45]. As the water strongly binds to the hydrophilic surfaces, it gives rise to repulsion that can significantly exceed the magnitude of the EDL forces. The exponentially decaying repulsive hydration forces have been experimentally measured for calcite [29, 41], mica [42, 43, 94], and silica surfaces [95] and could be generally characterized with decay lengths D_H < 2 nm [92]. Although the theoretical origin of the hydration forces (F_H) is still debated [96], they can be approximated using the exponential force law [92]:

$$F_H/R = Ce^{-D/D_H} \quad \text{(Eq. 11)}$$

where R is a radius of a sample curvature, C (mN/m) is an experimentally measured force constant and D is surface separation. Based on the different nature of hydration forces between two silica or two mica surfaces, a distinction has been made between the primary and secondary hydration forces. The much-shorter ranged primary hydration repulsion (D_H < 0.5 nm) typical for silica is due to the direct adsorption of water on protruding surface groups, while the longer-ranged (D_H < 2 nm) secondary hydration typical for mica is related to the hydration of counterions adsorbed onto mineral surfaces [92]. It has been found that the secondary hydration forces between mica surfaces depend on ion concentration but are also strongly ion-specific: the decay

lengths of hydration forces were larger for divalent Ca^{2+} and Mg^{2+} cations (~ 2 nm) than for monovalent cations (~ 1 nm), but the repulsion was the strongest for Na^{+} [42, 43, 45, 92]. This provides a possibility to modulate the secondary hydration by changing the composition of the fluid.

Ion correlation forces are short range attractive forces that become especially important in the presence of multivalent ions such as Ca^{2+} [97]. Ion correlation attraction has been suggested to cause a strong adhesion of clays in the presence of Ca^{2+} [98]. There has been no simple force law proposed to quantify the ion-correlation forces yet. However, this interaction has been suggested to originate due to the fluctuations in the density of mobile counterions in the EDL and can be thought of as a Van der Waals-like attraction of double layers [45, 99].

2.4 Surface forces between calcite surfaces

Although the forces between calcite surfaces have been indirectly measured in many colloidal calcite-based systems (mainly in the presence of organic molecules), there have been only a few works in which the forces between two calcite surfaces [44, 93, 100] or calcite-silica [25, 41] surfaces in aqueous solutions have been directly measured, using Atomic Force Microscopy (AFM).

Pourchet *et al.* (2013) [100] have observed a strong adhesion between two smooth calcite crystals in highly alkaline solutions (pH = 12), which has been attributed to the weaker EDL repulsive force at low calcite surface charge. On the other hand, Røyne *et al.* (2015) [44] have measured short-range (<5 nm) repulsive forces between two freshly cleaved single calcite crystals in water, which exceeded the theoretically-predicted EDL forces. This repulsion has been attributed to hydration forces acting between the hydrophilic calcite surfaces. Diao & Espinosa-Marzal (2016) [41] have measured the forces between single calcite surface and a colloidal silica probe in $CaCl_2$ electrolyte with varying concentration. The repulsive hydration forces they have observed, displayed an oscillatory behaviour, related to the squeezing of the hydrated counterions out of the contact region. Interestingly, the range of these hydration forces was decreasing with the increasing electrolyte concentration. The forces between two calcite surfaces have been later measured in NaCl electrolyte with varying ionic strength by Javadi & Røyne (2018) [93]. Only repulsive forces were measured at low ionic strengths (< 0.1 M), but adhesion could be observed at higher electrolyte concentrations. The collapse of hydration layers on the calcite surfaces and ion-correlation at higher electrolyte concentrations have been proposed to explain these observations.

Calcite is a mineral with a relatively low surface charge [101, 102] and only relatively weak EDL forces are expected to act between calcite surfaces. However, the experimental data has shown that strongly repulsive hydration forces may additionally act between calcite surfaces in low concentration electrolytes. The sensitivity of the hydration repulsion to the electrolyte concentration indicates that the hydration is most likely related to the presence of hydrated counterions adsorbed onto the calcite surfaces [41].

Experimental and modelling studies of the isolated calcite-water interfaces suggest an unconventional interfacial structure where two layers of water molecules are directly adsorbed to the calcite surface. The counterions are not bound directly to the surfaces but to these water layers as outer-sphere species [103-106]. As the disjoining pressure in the surface-adsorbed water film is very high [107] and the film is very thin (a few Å), it is not likely that it can give rise to the long-range repulsive force with a range of several nm. This supports the interpretation that the repulsive forces measured in the AFM experiments [41, 44] have been most likely related to the dehydration of outer-sphere adsorbed species upon squeezing them in a confined region between two surfaces. Adhesion between calcite surfaces has been observed at higher electrolyte concentrations or in high pH electrolytes. These findings suggest that at these conditions, the dehydration energy of the counterions adsorbed onto calcite is lower.

2.5 Roughness in surface force measurements

Surface roughness affects all forces that act between surfaces. This is because of the variation in surface heights across the contact area, and because of the reduced real area of contact with respect to the nominal contact area defined by the geometry of the surfaces. A rough topography affects the distribution of ionic species both adsorbed onto the surface and located in the EDL.

One approach to estimating these roughness effects is to average the total interaction energy (G) between two surfaces with respect to the distribution of surface heights in the contact region [108, 109]. The distribution of surface heights can be measured with the AFM. Using the model proposed by Parsons et. al. (2014) [108], the 'roughness-averaged' force ($F_{non-contact}$) can be estimated as:

$$F_{non-contact} = 2\pi R * \frac{1}{N_1 N_2} * \sum_i \sum_j H_{1i} * H_{2j} * G\left(h_{2j} - h_{1i} - \bar{h}_2 + \bar{h}_1 + D\right) \quad \text{(Eq. 12)}$$

where N_1 and N_2 are normalization factors ($N_1 = \sum_i H_{1i}\,; N_2 = \sum_j H_{2j}$), H_{1i} is a histogram of surface heights h_{1i} of the first surface, with a mean height value $\bar{h}_1$, and H_{2j} is the histogram of the second surface, and G can be any interaction energy between the surfaces, such as DLVO, hydration force, or a sum of these two. G is related to force F as $F = 2\pi RG(D)$ using the Derjaguin approximation. Histograms of surface heights can be for example obtained from AFM topography measurements.

The above expression treats the effect of roughness away from the surfaces. There is also another roughness effect which is related to the mechanical deformation of surface asperities. This effect is present when the surfaces are being placed in contact. Once the asperities of rough surfaces start to contact each other, they deform elastically or plastically. Since energy is needed to deform the asperities, this always produces a repulsive force. If the surfaces have a random distribution of surface heights, the force is exponentially repulsive. The effects of this mechanical contact force are present at separations ~3 rms, where rms is the root-mean-square roughness of the surface. As proposed by Parsons *et al.* (2014) [108], the mechanical repulsive force can be estimated from:

$$F_{contact} = \frac{4RE_r\sigma_m}{15\sqrt{\pi}}\sqrt{\frac{\sigma_m}{r_a}}exp\left(-\frac{D^2}{4\sigma_m^2}\right) * f\left(\frac{D}{\sigma_m}\right) \qquad \textit{(Eq. 13)}$$

where E_r is a reduced Young's modulus ($\frac{1}{E_r} = \frac{1-\nu_1^2}{E_1} + \frac{1-\nu_2^2}{E_2}$) with Young's modulus E and Poisson's ratio ν of surface 1 and 2, respectively; r_a is an average reduced radius of surface asperities ($\frac{1}{r_a} = \frac{1}{r_1} + \frac{1}{r_2}$) of surface 1 ($r_1$) and 2 ($r_2$); σ_m is the mean rms roughness of the surfaces ($\sigma_m = \sqrt{\sigma_1^2 + \sigma_1^2}$); and $f(x) = \sqrt{x}[(1 + x^2)K_{0.25}\left(\frac{x^2}{4}\right) - x^2K_{0.75}\left(\frac{x^2}{4}\right)]$, with K_n representing two modified Bessel functions of the second kind with $n = \frac{1}{4}$ and $n = \frac{3}{4}$. If the surfaces are very rough, the contact force may be sufficient to overcome adhesive VdW effects. Since the mechanical force is exponentially repulsive, it can be misinterpreted with any other exponentially repulsive interaction such as hydration force or even EDL repulsion. This is especially important in force measurements with reactive surfaces, such as calcite, which may become rough in contact with aqueous solutions during the force measurements.

2.6 Reactivity of calcite in confinement

A topic that has not yet been explored is how surface forces between calcite surfaces are affected by calcite reactivity in contact with water or electrolyte solutions. Equally interesting is

how the calcite reactivity is influenced by a spatial confinement. The most important effects of confinement on the reactivity of minerals are the following:

- Confinement restricts the transport of ionic species in the solution. In solutions supersaturated with respect to a crystal, this may produce rough rim topographies at the edges of a growing, confined crystal face. The growing edges consume the solute and cavity develops in the center of the confined face, where the growth is slower because of the solute depletion [110, 111].
- Higher supersaturations are needed to nucleate a crystal in confinement, relative to a bulk solution, because ion depletion and reduced ion mobility make the nucleation less probable [112, 113].
- Confinement may prevent the crystallization completely if the pore dimensions are smaller than the critical nuclei size. In that case, the growth may be prevented due to the surface free energy barrier [114].
- A higher density of ionic species near charged pore surfaces may promote the growth of the otherwise unstable phases [115].

It is intuitive to think that most of the confinement effects are present when the separation between the surfaces or the dimensions of pores are of the order of nanometers. However, a recent study by Stephens *et al.* (2013) [55] have shown that even μm-range confinement can significantly affect the crystallization of calcium carbonate. They have observed that ACC can be stabilized between two surfaces separated by 1 μm, while calcite only nucleated at larger separations in the same solution conditions. The observed stabilization of ACC was attributed to kinetic effects related to restricted ion transport in the confined solution.

2.7 Calcite in materials

Calcite is not only important in geological environments, but it is also one of the most commonly used mineral resources. It has been estimated that over 4 billion tonnes of carbonate rocks are mined worldwide annually [116]. Only a small proportion of these rocks is used directly after mining, mostly in construction. The rest of the rocks undergoes more thorough processing. The first processing step, which is crushing and grinding, provides a raw carbonate material used in road construction, metallurgy, fertilizer production, flue gas desulphurization, glass and ceramics, and some types of concrete. The second processing step involves calcination during which the ground raw material is decomposed at temperatures above 800 °C:

$$CaCO_3 \xrightarrow{heat} CaO + CO_2(g)$$

Most of the calcined material (lime) is then used for cement production and some part of it is used in the chemical industry. The third processing step involves a controlled reprecipitation of lime back to calcium carbonate, in order to obtain a high purity precipitated calcium carbonate (PCC) with controlled particle size:

$$CaO + H_2O \rightarrow Ca(OH)_2$$

$$Ca(OH)_2 + CO_2(g) \rightarrow CaCO_3 \text{ (PCC)}$$

PCC is used mainly as a filler in plastic, paper and paint production, and as an excipient in pharmaceutical products. In many cases PCC is coated with a small amount of organic molecules, such as fatty acids, to improve its dispersibility as a filler in solvents and polymer melts [116].

Calcium carbonate is mainly used as a pigment or filler, usually with no advanced function itself. However, since $CaCO_3$ is already used in large quantities in many industrial processes, a large potential exists to improve the properties of $CaCO_3$ based-materials by adjusting the surface chemistry of $CaCO_3$. There is a large interest in calcite-based colloidal systems in which repulsive or adhesive interaction between calcite surfaces is required, mainly in relation to polymers, surface coatings, cement, and mineral flotation [117-119].

Many inorganic fillers, including $CaCO_3$, have been demonstrated to improve the mechanical properties of polymers, which has motivated a lot of research (e.g. [120-123]). In many cases, uncoated calcite particles have been shown to have an adverse or no effect on the mechanical strength of polymers [123], which could be attributed to the uncontrolled aggregation of crystals within the polymer volume [120]. On the other hand, when calcite particles were coated with organic molecules, they have been observed to improve the mechanical properties of polymers [124]. This effect was most effective when the molecules comprising the surface coating could strongly interact with the functional groups of the polymers [124-126]. Thus, the organic molecules that can effectively bind both to the calcite filler phase and to the polymer should be the most efficient to enhance mechanical properties of calcite-polymer composites.

Surface coatings and paints are multicomponent mixtures, in which the possible role of $CaCO_3$, apart from being a pigment, is to improve cohesion, adhesion to surfaces, emulsion stability and its rheological properties [116, 127]. It has been observed that it is possible to prepare surface coatings with fair rheological properties with as much as 70 weight % of $CaCO_3$ [127]. However, the calcite particles must be first covered with the organic dispersant sodium

polyacrylate (which due to the presence of carboxylic groups in its chain, has a high affinity to adsorb on calcite [128]).

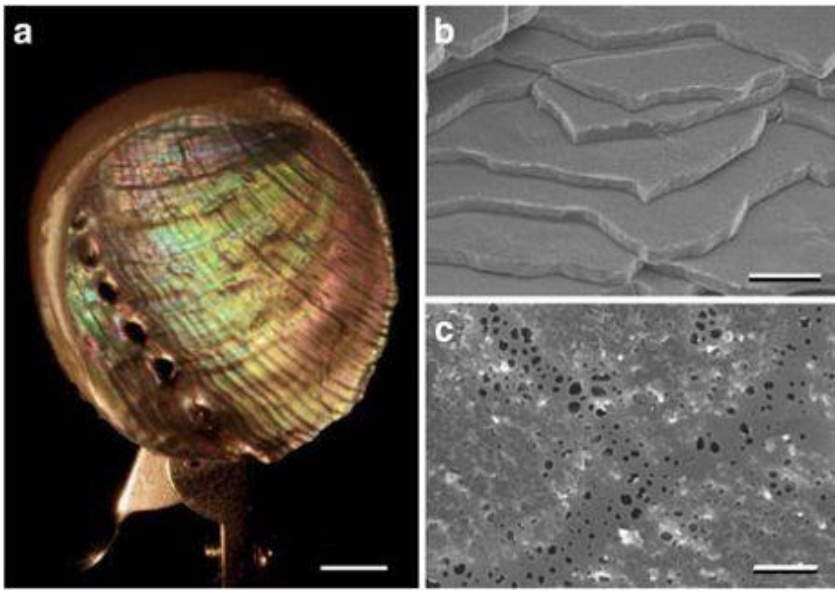

Figure 8. *Images of a) nacre biomineral (scale bar 5 mm); b) stacked calcium carbonate platelets comprising nacre (scale bar 2 μm); c) porous organic layer in nacre that allows for a crystal continuity in vertical direction between plates (scale bar 500 nm). Image originally from Finnemore et al., Nature communications 3 (2012): 966 [132].*

There have not been many such attempts to obtain materials where calcite is the dominant phase. A substantial amount of fine limestone (< 20 weight %) can be added to cement formulations [129]. Limestone grains can increase the cement cohesion and plasticity in the presence of dispersing agents such as sodium polyacrylate or polyphosphates. This effect is strongly related to particle sizes, and its mechanism is mainly based on the improved close-packing of grains within the cement. The variability of particle sizes often leads contradictory conclusions as to whether the presence of limestone improves the properties of cement [129-131].

In conclusion, even though calcite is commonly used in numerous materials, there are few examples of formulations in which calcite is the dominant phase. On the other hand, marine organisms are excellent in synthesizing advanced $CaCO_3$-based biomaterials that act as robust and strong shells, gravity sensing systems, lenses, or skeletons. One example is nacre, which is a composite made of ~ 500 nm-thick inorganic platelets of calcium carbonate and < 100 nm-thick organic layers of polysaccharides and proteins in between [132]. The plates are intergrown with each other through the holes in the organic layers (**Figure 8**). This structure makes the nacre especially strong and prevents a transverse crack propagation. Artificial nacre has been

successfully synthesized in laboratory experiments [132]. Such inorganic-organic composites can inspire possible ways to modify surfaces of commonplace calcite fillers [133].

2.8 Interaction of organic molecules with calcite surfaces

As has been discussed in many places in this thesis, the interaction of calcite with organic molecules plays an important role for living organisms, materials and geological environments. There is a great number of experimental and modelling studies which have investigated the adsorption of small or polymeric organic molecules onto single calcite surfaces (e.g. [134-144]).

Calcite is an ionic crystal composed of Ca^{2+} and CO_3^{2+}. On the calcite surface, there are undercoordinated O and Ca atoms. Since the number of the negatively (O) and positively (Ca) undercoordinated atoms is the same per unit cell, the surface has no net charge. However, there is a local partial positive charge on uncoordinated Ca atoms and local negative partial charge on uncoordinated O atoms, which drives the adsorption of species on calcite surface [142]. In water, there are undissociated water molecules bound to the surface atoms [145], and other ionic species in the solution can bind as outer sphere complexes indirectly to these water molecules [106]. Organic species with polar functional groups can generally bind strongly to calcite surfaces by two main mechanisms: electrostatic interaction between surface Ca atoms and electronegative O atoms in organic molecules, and by hydrogen bonds between H atoms of organic molecules and O atom on calcite surface [142]. If one organic molecule can form these two bonds at the same time, or if it can form several bonds via its several functional groups, then the adsorption energy for such molecule is larger than for a single bond [134, 136, 142]. In this case, the mutual positions of functional groups determine the strength of the adsorption [138]. Sometimes molecules cannot be adsorbed strongly to surfaces for steric hindrance reasons.

According to many studies, carboxylic $-COOH$ functional groups have the highest affinity to adsorb on calcite surfaces, with adsorption energies higher than molecules with hydroxyl $-OH$ or with aldehyde $-CHO$ groups [134-140, 142-144, 146]. Carboxylic groups adsorb on calcite surfaces by complexation of the positively charged calcite surface $-Ca^{+}$ sites by carboxylate oxygens [134]. The adsorption has been found to be stronger for dicarboxylic acids and for larger molecules with several carboxylic groups [134, 139]. A consequence of the strong adsorption of carboxylic acids on calcite is passivation of calcite surface, which prevents dissolution and delays calcite growth [135, 140]. Passivation of calcite surfaces has been also observed for many other organic molecules that can adsorb onto calcite [147].

What remains unknown is how two calcite surfaces will interact with each other in the presence of strongly-adsorbing organic molecules. There have been force measurements in which

the interaction of $-COOH$ groups with single calcite surfaces was investigated [77], or measurements in colloidal calcite systems with the use of dispersants with carboxylic groups [119], but such experimental data is limited. It is also not clear how the adsorption of dicarboxylic acids is affected by the surface roughness, where the distribution of partial charges on calcite surface is different than for the smooth surfaces. Forces between two rough calcite surfaces in the presence of dicarboxylic acid molecules were investigated in this thesis using the Surface Forces Apparatus (Manuscript 3).

CHAPTER 3

EXPERIMENTAL METHOD

3.1 Force measurements with the Surface Forces Apparatus

The main goal of this experimental thesis was to measure the forces between two calcite surfaces in aqueous solutions of varying compositions. All force measurements were performed using the Surface Forces Apparatus (SFA). There is a plenty of force-measuring techniques which can measure forces in an indirect way, such as particle detachment experiments, peeling experiments, measurements of the colloidal stability of dispersions, and more [45]. Only a few of them allow measurements of the full force interaction, which means that the forces are measured as a function of the separation between two surfaces. SFA is among few direct force measuring techniques that provide a full force-distance interaction and the absolute separation (D) between the surfaces [45, 148-150]. Another great benefit of the SFA is that it gives *in situ* information about the contact topography [151].

Figure 9 shows a schematic representation of the SFA setup. Forces $F(D)$ acting between two surfaces during the SFA measurement are calculated from the deflection of a force measuring spring (with a spring constant k). The base of the spring is moved vertically up on loading or down on retraction by a known distance ΔD_A. During the loading-unloading cycles, at large separations (where the $F(D) = 0$), a change in the separation between the surfaces ΔD is equal to a displacement of the spring base ΔD_A. At smaller separations, there may be some force acting between the surfaces. If at a given separation D, the force $F(D) \neq 0$, the spring deflects, and the

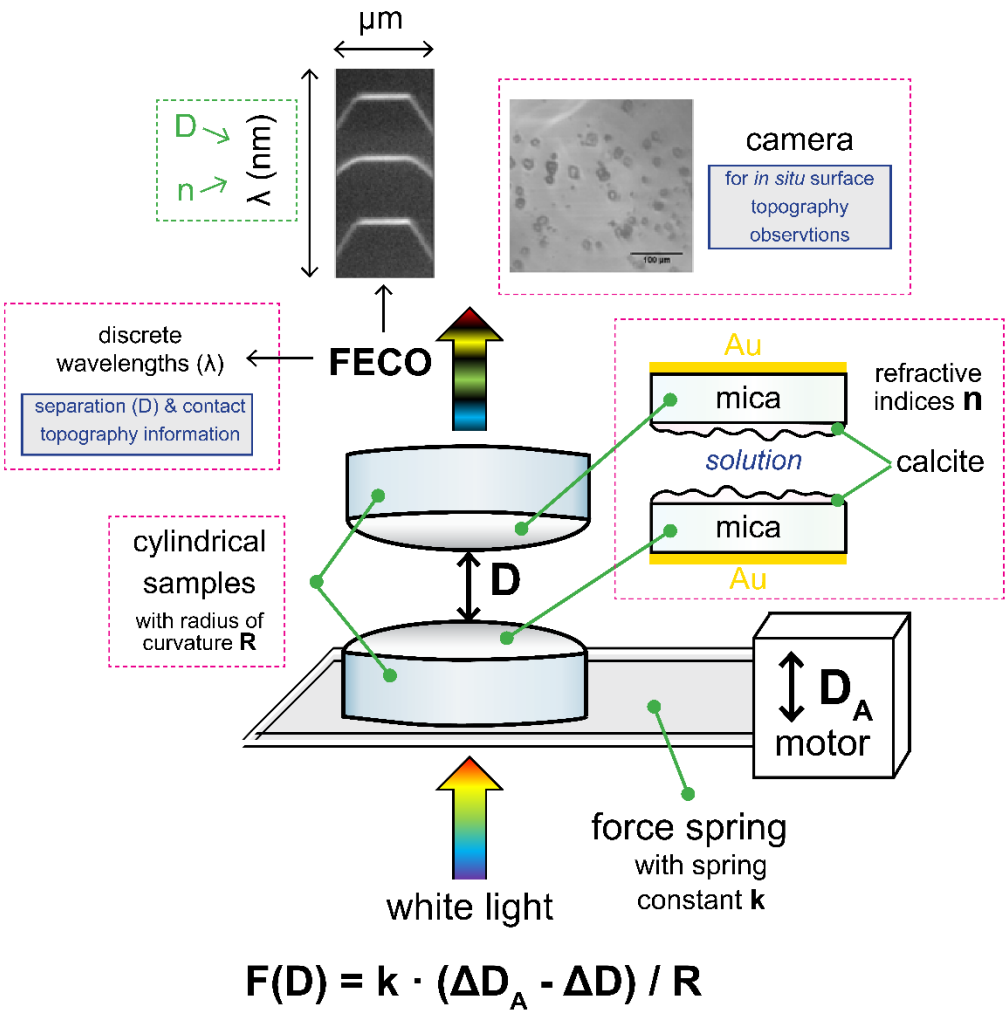

***Figure 9**. Schematic representation of the Surface Forces Apparatus setup (FECO - fringes of equal chromatic order). The nominal contact area between the surfaces is ~0.03 mm² for the cylindrical samples with the radius of curvature R = 0.02 m.*

change in the separation between the surfaces is no longer equal to the displacement of the spring base ($\Delta D \neq \Delta D_A$). The force $F(D)$ can be calculated as:

$$F(D) = k(\Delta D_A - \Delta D) \qquad (Eq.\ 14)$$

While the spring base displacement ΔD_A is known, SFA has to be coupled with another technique to measure the absolute separation between the surfaces (D), and calibrate the spring base movement. Most frequently, SFA is coupled with an optical interferometric technique: Multiple Beam Interferometry (MBI) [152-154]. In MBI, a white light beam is passed through the two

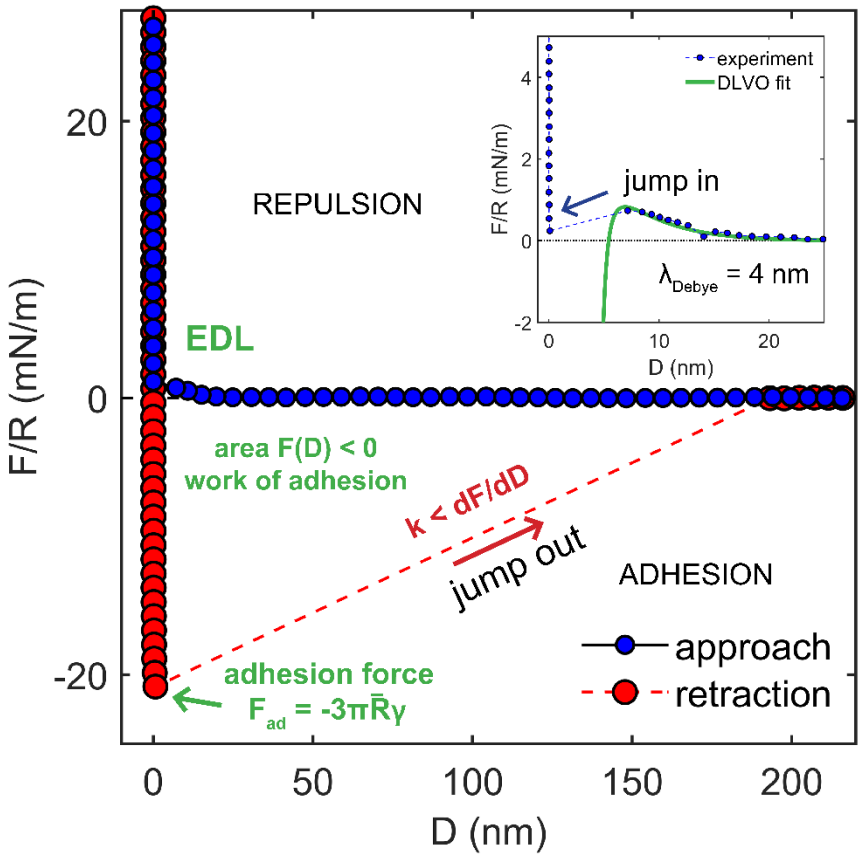

Figure 10. *Exemplary SFA measurement of the force (F) as a function of separation (D) for two mica surfaces in 5 mM NaCl solution (pH 3; Debye length λ_{Debye}= 4 nm). The inset zooms on separations D < 25 nm for the force curve on approach. DLVO fit was calculated using Eq. 5, 7 and 9 and the Hamaker constant for two mica surfaces in water A = 2.2·10^{-20} J [43]. Adhesive jump in and jump out instabilities occur when the spring constant k is lower than the maximum slope of force-distance curve. Adhesion force is the minimum force measured on retraction and can be related to the surface energy γ as indicated on the plot ($\bar{R} = R^2/2R$, where R is the radius of SFA sample curvature; see equation 12.10 in Israelachvili [45]).*

opposing SFA samples (see **Figure 9**), undergoes multiple reflections between the surfaces, emerges as a set of interference FECO fringes (fringes of equal chromatic order) at discrete wavelength positions, and is directed to the spectrometer. The wavelength (λ) positions of the FECO depend on refractive indices (n) and thicknesses of all the layers that comprise the SFA samples. For the MBI to work, the SFA samples must be transparent and semi-reflective. Transparency of a mineral sample is usually achieved by making it very thin (< 10 μm). To make the sample semi-reflective, a thin layer of metal (~55 nm Ag or Au) is deposited on one side of the sample. In a typical SFA experiment with mineral surfaces, the sample most often comprises an

Ag-mineral-solution-mineral-Ag interferometer. Usually, refractive indices and thicknesses of all the layers are known, apart from the thickness of a solution film, which is equal to the separation D between the two surfaces. D can be then easily calculated using the available analytical solutions for a given interferometer [154]. Some part of the transmitted light is also directed to the camera for the surface topography *in situ* observations. Typical distance resolution of the SFA is 1 Å. **Figure 10** shows an exemplary force-distance curve measured with the SFA between two smooth mica surfaces in an adhesive system (5 mM NaCl, pH = 3 solution).

Since FECO fringes are sensitive to the distance between two surfaces, they also provide *in situ* information about sample topography in the observed contact region. This is very useful when following changes in roughness of reactive solid samples. Additionally, as the position of FECO fringes depends on the refractive indices of the layers, they can provide information about precipitation of new phases on the surface of solid samples, or about nucleation taking place in the solution. An exemplary FECO pattern of two smooth surfaces in contact is shown in the top part of **Figure 9.** Whereas vertical wavelength (λ) positions of FECO correspond to the separation between surfaces, the shape of FECO in lateral direction corresponds to the shape and size of the contact. The flattened part of FECO (~ 100 μm) marks the contact region because the surfaces flatten in contact elastically under the applied load (or due to strong adhesive forces; see chapter 12 in Israelachvili [45]). The lateral resolution of FECO is ~ 1 μm.

Because of a cylindrical geometry of the SFA samples and their quite large radius of curvature (R = 0.02 m), the nominal contact area in the SFA is ~0.03 mm^2. This is much larger than in standard AFM experiments and allows a measurement of how two macroscopic surfaces interact at small separations. Additionally, if the surfaces are reactive, SFA can give an insight into the solid reactivity and recrystallization in confinement, since the separation between the surfaces is < 10 μm for a ~1 mm^2-large area [55].

3.2 Using calcite in the Surface Forces Apparatus

SFA is commonly used to measure forces between mica surfaces, and less often between other mineral surfaces such as silica, quartz, gypsum or sapphire [43, 155-157]. Mica is the most common substrate in the SFA because it is atomically smooth and can be easily cleaved into thin (< 10 μm) and flexible films. It is thus simple to glue the cleaved mica onto the SFA samples with a cylindrical curvature. Apart from the results presented here, to the best of my knowledge, there has been no prior force measurements with two calcite surfaces in the SFA. Chen *et al.* (2017) [158] used discontinuous calcite substrates (with single calcite crystals grown on mica) in the SFA, but only in order to follow calcite reactivity.

We tested three ways of mounting calcite samples in the SFA:

- Using flat, cleaved and polished single calcite crystals with thickness < 10 μm. This only worked in a sphere-on-flat SFA geometry, rather than in the standard crossed-cylinders SFA setup. We could successfully mount single crystal calcite surfaces in the SFA after polishing them to thicknesses << 10 μm. However, we could only use one calcite (flat) surface against mica surface (on a spherical SFA disk).

- Using $CaCO_3$ films precipitated using the PILP method [159], in which thin calcite films grow on a solid substrate (e.g. mica) in the presence of a soluble organic polymer additive. We tested the growth of PILP-calcite films on glass or mica substrates. However, this method yielded discontinuous $CaCO_3$ films, likely with traces of the incorporated organic phase.

- Using Atomic Layer Deposition (ALD) method, in which polycrystalline 200 nm-thick calcite films can be deposited on a solid substrate from the vapor phase. We deposited calcite films on thin, cleaved mica substrates, and thus we could easily glue the samples to the cylindrical SFA disks (**Figure 9, Figure 1** in Manuscript 1). Details of the ALD deposition method have been described in Nilsen *et al.* (2001) [160]. The detailed description of how to prepare the ALD-deposited calcite samples for the SFA measurements is presented in Manuscript 1 [161]. Briefly, during the ALD deposition process, calcite film precursors are sequentially pulsed into the reaction chamber. Since between each pulse of the precursors an inert gas (N_2) is purged into the ALD chamber, the growth is eliminated in the gas phase, and it can only occur on the solid substrate (in our case on mica) [160]. The precursors used to grow the ALD calcite films in this work were: $Ca(thd)_2$ (Hthds2,2,6,6-tetramethylheptan3,5-dione) as a source of Ca, ozone and CO_2 [160] The deposition temperature varied between 250 and 300 °C.

As our goal was to perform SFA force measurements between two calcite surfaces, the ALD deposited calcite films were the most suitable: It was possible to attach them to curved, cylindrical SFA disks and they were continuous over the whole surface of the samples (cm^2-large areas). X-ray diffraction (XRD) analysis was performed after each deposition to confirm that the films were composed of calcite (see **Figure 3** in Manuscript 1, **Figure S10** in Supporting Information for Manuscript1, and **Figure S1** in Supporting Information for Manuscript 2). The major drawback of the ALD polycrystalline calcite surfaces was the poorly controlled surface roughness. The

roughness varied between each ALD deposition and sometimes also across samples deposited in a single ALD run. As such, if possible, the sets of SFA measurements were performed using calcite surfaces prepared in one ALD deposition run, in order to limit the variation in roughness. The roughness of the ALD samples was measured with AFM on dry samples before and after the SFA experiments. The AFM roughness data is of all the used ALD films is presented and discussed in Manuscripts 1 and 2 (e.g. **Figure 4** in Manuscript 1, **Figures S4** and **S5** in Supporting Information for Manuscript 2). **Figure 11** below shows exemplary Scanning Electron Microscopy (SEM) image of an ALD calcite film and an AFM height map measured for the same sample.

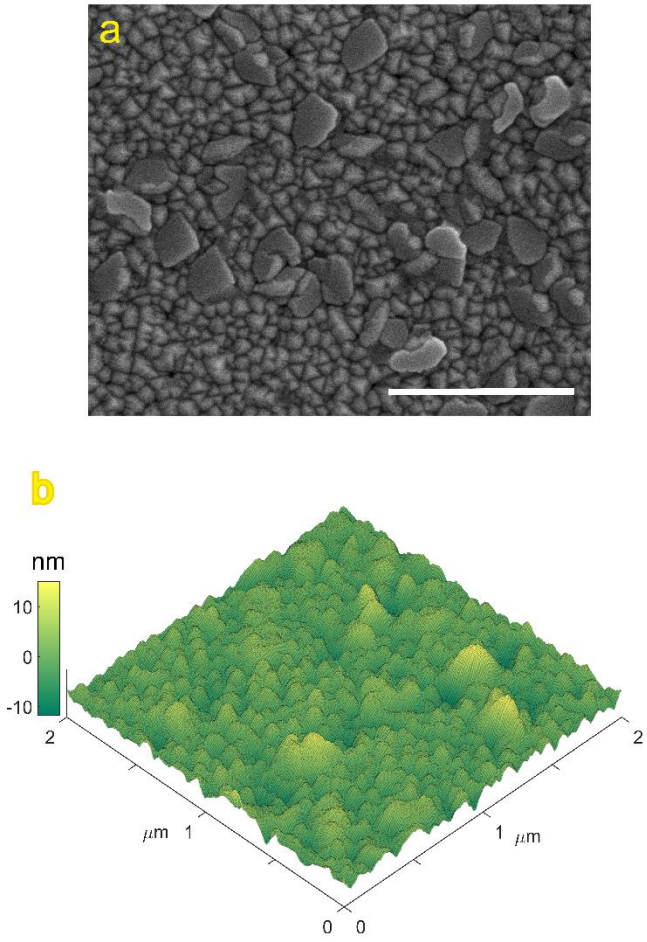

Figure 11. *Topography of ALD calcite films: a) SEM image (scale bar 1 μm); b) AFM height map. The rms roughness of the sample is 3 nm.*

3.3 Data analysis with Reflcalc

A separation between surfaces (D) in the SFA is typically calculated from the wavelength (λ) positions of FECO interferometric patterns. The FECO λ positions depend on the refractive indices (n) and thicknesses of all the layers that comprise SFA samples (including the water film trapped between the surfaces). In a typical SFA experiment, samples consist of back-silvered mica layers that comprise a three-layer *mica-water-mica* interferometer. Single mica crystals are cleaved into thin layers in order to assure their uniform thickness [162], which greatly facilitates the analysis of the interferometric FECO patterns: Simple analytical solutions are available to calculate separation between two mica surfaces immersed in water, which only require that the refractive indices of mica and aqueous solution are known [154] (see also **Eq.S1** in Supplementary Information for Manuscript 1). However, the analytical interferometer solutions are most adequate for the SFA experiments in which the position of the contact fringes is known, the maximum separation between the surfaces is relatively small (< 200 nm), and the number of layers comprising samples is small.

Analysis of the FECO patterns is more complex when using multilayered and unsymmetrical interferometers such as our ALD calcite surfaces (see **Figure 9**). Analytical solutions are not suitable for our system, especially because the separation between rough and reactive calcite surfaces may change from small, nm-range to large, μm-range distances within one SFA experiment. Therefore, in order to calculate separation between two calcite surfaces in this work, we used an alternative approach which is the modelling of FECO λ positions using the open source software Reflcalc [163]. Reflcalc uses the matrix method for stratified samples adapted from Schubert [164] in order to calculate the light transmission through multilayered samples. A large number of thin solid or liquid layers can be used in the modelling. The input parameters in Reflcalc modelling are material-characteristic optical parameters (refractive indices and extinction coefficients) and thicknesses of each layer comprising the samples. To determine the correct surface separation for each measured data point during SFA force measurements, the Reflcalc-modelled λ positions of FECO are compared with the FECO λ positions measured during experiments. This analysis was performed in the MATLAB software, as described in detail in **Section S1** of the Supporting Information for Manuscript 1.

Our Reflcalc-MATLAB analysis was compared with the standard analytical solution for three typical SFA mica-mica experiments in aqueous solutions (see **Section S1.4** of the Supporting Information for Manuscript 1). We found a good agreement between these two methods of the SFA data analysis. One can, however, expect additional sources of error in the determination of separation between the surfaces when using rough and inhomogeneous calcite

surfaces. These mainly involve: misestimation of calcite thickness, which varies in different locations on a sample; changes in calcite thickness during experiments due to calcite reactivity in contact with solutions that are not accounted for in the analysis; and broadening of FECO fringes because of the increasing roughness of calcite layers during the experiments. A more detailed discussion regarding these possible sources of error in the determination of the separation between calcite surfaces is presented in **Section S1.5** of the Supporting Information for Manuscript 1. We estimate that the error in the determination of absolute surface separation can in some cases be as large as 100 nm, but the relative error between the consecutive data points in SFA force-distance curves should be << 100 nm.

CHAPTER 4

SUMMARY OF MANUSCRIPTS

4.1 Manuscript 1:

Forces between rough and reactive calcite surfaces in calcite-saturated water

The first article titled '*Surface Forces Apparatus measurements of interactions between rough and reactive calcite surfaces*' addresses the forces acting between two calcite surfaces or calcite and mica surfaces in water that has been saturated with respect to calcite.

We measured monotonically repulsive forces between two rough and polycrystalline calcite surfaces in the saturated water. This was in line with the previous findings of Røyne *et al.* (2015) [44] and Diao & Espinosa-Marzal (2016) [41], who have measured repulsive forces between two calcite or calcite and silica surfaces, and attributed this interaction to the repulsive hydration forces. In our system, the forces were affected by the nm-scale roughness of the polycrystalline calcite surfaces. We addressed the effect of roughness by semi-quantifying it according to the model proposed by Parsons *et al.* (2014) [108]. Our results show that both the effect of roughness and the repulsive hydration force gave rise to the exponentially decaying repulsion. The hydration repulsion is a much shorter-ranged interaction than the roughness-related mechanical force. Nevertheless, it was not possible to separate these two contributions unambiguously due to the lack of precise information about the roughness in the contact region. We additionally observed that the magnitude and range of the measured repulsion were changing with time, which was attributed to the roughening of calcite surfaces in water. In some cases,

during the force measurements between two calcite surfaces, we observed an additional strong repulsion related to the nm-scale surface recrystallization in the contact region. This repulsive 'force of crystallization' could overcome the confining pressures of the order of MPa (which was estimated assuming that the real contact area was a very small fraction of the nominal contact area). Our findings were discussed in the context of the water-weakening phenomenon in carbonates. We suggested an additional mechanism in which even the nm-scale recrystallization of confined calcite surfaces in contact with water may bring about a strongly repulsive force of crystallization, and as a result, cause the decrease in cohesion between the individual calcite grains that comprise the rock.

In this work, we additionally measured the forces in an asymmetric system, between one rough calcite and one smooth mica surface in calcite-saturated water. In several experiments, the calcite surfaces were smooth enough to measure the adhesive forces in this surface configuration (as the real contact areas were relatively large). If present, the magnitude of adhesion varied with the time and was becoming larger in consecutive force-distance measurements (during which the surfaces were repeatedly approached and retracted from each other). We attributed this increase in adhesion to the growing real contact areas. This process was driven by pressure solution or plastic deformation of the highest asperities on the calcite surface, under the repeatedly applied load. If the surfaces were kept in contact under the constant applied load for several hours, the contact topographies were becoming rougher.

Moreover, based on the control experiments between two mica surfaces in the same solution, we suggested that the measured adhesion between mica and calcite surfaces could not be solely attributed to Van der Waals forces, and that the electrostatic attraction between positively charged calcite and negatively charged mica could have contributed to the measured adhesion. These findings have interesting implications for the enhanced pressure solution phenomena that has been observed in the presence of clay minerals [46]. Our work indicates that the contacts between mica and calcite should be stronger than between two calcite surfaces. If the surface forces play a major role in pressure solution, then mica should not enhance pressure solution of calcite, as these two minerals should form strong adhesive contacts.

4.2 Manuscript 2:

Forces between rough and reactive calcite surfaces in calcite-saturated electrolyte solutions

In Manuscript 2, titled '*Nucleation in confinement generates long-range repulsion between rough calcite surfaces*', we investigated the forces between two polycrystalline and rough calcite surfaces in electrolyte solutions with varying composition and ionic strength. The importance of such study is related to the strongly varying levels of salinity of pore waters that saturate sedimentary rocks [165]. Moreover, according to the observations of Javadi & Røyne (2018) [93] and Pouget *et al.* (2013), adhesive forces between calcite surfaces can be measured in concentrated electrolyte solutions (> 0.1 M). In our system, we additionally examined the effect of roughness and surface reactivity in confinement on the measured forces. Although adhesive forces can act between calcite surfaces at higher electrolyte concentrations, this effect might be counteracted by the repulsive forces associated with calcite recrystallization, which may be locally driven in these concentrated solutions.

We did not measure any adhesive forces, which were expected to act between calcite surfaces in concentrated electrolyte solutions. Only monotonically repulsive forces were present in all NaCl, $CaCl_2$ and $MgCl_2$ solutions, even when the solution ionic strength was as high as 1M. In most of the experiments, we observed a sudden increase in the range and magnitude of the repulsion. This increase was correlated with the nucleation of an amorphous or poorly crystalline precipitate in the contact region. The precipitate did not form heterogeneously on the calcite surfaces but formed in the confined solution, and it was most likely a hydrated and viscous $CaCO_3$ phase. Because the precipitate persisted in the gap between the two surfaces, it gave rise to the long-range and high-magnitude repulsion acting between two calcite surfaces. We suggest that this repulsion was of a hydrodynamic origin. The magnitude and range of the repulsion were the largest the moment when the precipitate was spreading into the contact region. We associated this peak in the repulsive forces with the pressure that the growing precipitates exerted on the confining walls. The nucleation in the solution was significantly hindered in the presence of Mg^{2+}. We could not obtain any precise data about the phase and crystallinity of the precipitate *in situ* in the SFA, or after the experiments with AFM or SEM.

The observed phenomenon has important implications for surface forces acting between reactive surfaces, crystallization in confinement, transport of reactants in thin water films between mineral surfaces, intergranular cementation, and evolution of microstructures both in geological environments and in calcite-based materials. Importantly, our results indicate that the adhesion between calcite surfaces in high salinity solutions may be counteracted by the repulsive

forces associated with the recrystallization processes occurring in confinement. Such repulsion may in turn impact deformation processes in rocks and materials, which often starts at grain boundaries and in fractures where the solid phases are exposed to percolating fluids.

4.3 Manuscript 3:

Forces between rough and reactive calcite surfaces in aqueous solutions containing organic molecules

Manuscript 3, titled '*Effect of Ca^{2+} on forces between calcite or mica surfaces in presence of dicarboxylic acids*', addresses the interaction between rough and reactive calcite surfaces in dicarboxylic acid solutions. We used water-soluble dicarboxylic acids with a varying number of carbon atoms per molecule (2 to 7). Dicarboxylic acids have been previously shown to strongly adsorb onto calcite and passivate the calcite surface against dissolution [134]. In this work, we investigated whether these organic molecules can also strongly adsorb onto rough and polycrystalline calcite surfaces, influence calcite reactivity, and significantly affect the forces between two calcite surfaces.

Our results indicate that dicarboxylic acids did not strongly adsorb on calcite surfaces, as the surfaces were dissolving during the experiments. Also, we found little influence of the dicarboxylic on the forces between calcite surfaces measured in dicarboxylic acid solutions (pH = 8.2-8.4, 50 mM). We measured adhesive forces only in some of the experiments with the longer-chained adipic and pimelic acids, with 6 and 7 carbon atoms per molecule. The minimum of these adhesive forces was located far away from the contact position. Also, the adhesion was present only if the surfaces were strongly dissolving. Based on that, we suggested that the adhesion was related to the long-range hydrophobic attractive force between the organic molecules that could be weakly adsorbed to calcite, and/or to the presence of high amounts of Ca^{2+} in the solution confined between the dissolving calcite surfaces.

To exclude the effect of roughness, we performed control experiments between two smooth mica surfaces. The control experiments in Ca^{2+}-free solutions did not indicate that the long-range hydrophobic attraction acted between two mica surfaces in dicarboxylic acid solutions. Since in calcite-calcite setup, there was likely a substantial amount of Ca^{2+} due to the dissolution of calcite, we also measured forces between two mica surfaces in dicarboxylic acid solutions with the varying amounts of added Ca^{2+}. The forces were adhesive, and the magnitude of the adhesion was increasing with the increasing Ca^{2+} concentration. However, since clay surfaces are known to interact strongly with each other in the presence of Ca^{2+} (due to the attractive ion correlation forces), it was not clear if the organic molecules had any influence on the measured adhesion.

Our results indicate that small dicarboxylic acid with 2 to 7 carbon atoms in a molecule are not efficient to significantly modify the surface properties of rough calcite surfaces in our system. Dicarboxylic acids did not promote enhanced repulsion or any strong adhesion between our calcite surfaces in pH 8.2-8.4 aqueous solutions. Therefore, our results suggest that alone, dicarboxylic acids have little potential to change the surface properties of calcite in water-based colloidal systems.

4.4 Conclusions and Outlook

The main goal of this thesis was to investigate to what extent the nanoscale surface forces acting between reactive calcite surfaces in aqueous solutions may contribute to the macroscopic strength and cohesion of carbonate rocks and calcite-based granular materials. As such, it was important to investigate any possible feedbacks between the nm-range surface forces and calcite reactivity in aqueous solutions. **Figure 12** shows a schematic overview of the main processes studied between two confined calcite surfaces in the SFA experiments. These involved measurements in three types of aqueous solutions: calcite-saturated water, calcite-saturated electrolyte solutions, and aqueous solutions with dissolved dicarboxylic acid molecules. Apart from the nm-range surface forces between two calcite surfaces, we investigated calcite dissolution and recrystallization, surface roughening, precipitation in confined solution, and mechanical effects due to the deformation of surface asperities during repeated loading-unloading cycles. As the nominal contact area between calcite surfaces in SFA experiments is large (contact radius of 50-100 μm), all the recrystallization processes that we observed in the contact region occurred in confined solutions. Such a system is relevant for geological environments and granular calcite-based materials because many deformation processes often start in confined regions where solid surfaces are in contact with the percolating fluids.

Surface forces that we measured between two rough, polycrystalline calcite surfaces with the SFA in inorganic solutions were always repulsive. The roughness of the calcite surfaces largely contributed to the magnitude of the measured repulsion. Additionally, the recrystallization of calcite surfaces, even at nm-scale, further enhanced the magnitude and onset of the repulsive forces. The repulsive forces associated with both nm-scale surface roughness and surface recrystallization events may be much larger in magnitude than the repulsive hydration forces previously attributed to calcite surfaces [44]. According to the DLVO theory, most mineral surfaces, including calcite, should form strong adhesive contacts in concentrated electrolyte solutions due to the screening of electrical double layer repulsive forces [93]. Our measurements indicated no adhesive forces between calcite surfaces even in the most concentrated (1 M) salt

solutions. These findings suggest that the high roughness of mineral surfaces may prevent them from forming strong adhesive contacts, despite the fact that the corresponding smooth mineral surfaces would likely attract each other in a given aqueous solution. Moreover, once exposed to aqueous solutions, calcite surfaces are not likely to form very strong adhesive contacts in weakly basic solutions (pH 8-9), which can in part contribute to the water-weakening phenomenon in carbonate rocks. In contrast, we measured adhesive forces in an unsymmetrical system between smooth mica and calcite surfaces, provided that the calcite roughness was relatively low. We suggest that the measured adhesion was likely due to the electrostatic interactions between oppositely charged mica and calcite surfaces and that mica and calcite may form relatively stronger contacts than two calcite surfaces in geological environments.

We showed that substantial recrystallization of calcite surfaces may occur in confined spaces, also in solutions that are globally slightly undersaturated with respect to calcite. We suggest that such effects may be partially attributed to a high surface energy of rough calcite surfaces [56] but also to the spatial confinement, which may promote a local supersaturation with respect to calcite due to the relatively slow diffusion of ionic species out of the gap between the dissolving surfaces. Our observations show that the recrystallization of calcite surfaces in confined spaces may occur *via* an unexpected mechanism, in which the precipitates grew in the solution trapped between the surfaces but not directly onto the calcite surfaces (even if the gap between the surfaces was μm-thick). We suggest that this effect was related to the spatial confinement, which hindered dehydration of the poorly crystalline and liquid-like precipitate. We also showed that the presence of the viscous precipitate between calcite surfaces gave rise to the long-range and high-magnitude repulsive forces between the surfaces. As such, in slightly basic pH conditions (pH 8-9), recrystallization and growth of calcite in confined spaces in our system were rather displacive than cementing. The observed repulsive forces associated with the displacive recrystallization may have crucial consequences for the evolution of porosity and microstructure in rocks and calcite-based materials, especially in the context of the pressure solution and the water-weakening phenomenon, both commonly occurring in carbonate rocks. Additionally, precipitation in confined solution may influence the transport of reactants from the dissolution sites to the precipitation sites, which is a crucial step in pressure solution. Although we did not measure the transport of ionic species in our system, we suggest that the presence of viscous phase between the surfaces may significantly slow down the diffusion of ions even in relatively thick, μm-wide gaps between the surfaces.

The findings presented in this thesis show that rough calcite surfaces tend to form weak contacts in weakly basic pH solution conditions and that the growth and recrystallization of calcite

surfaces can enhance the magnitude and range of repulsive forces. In order to fully understand the link between the surface forces and recrystallization of calcite, the future work should involve force measurements between two calcite surfaces as a function of solution pH: It has been recently observed that calcite can form strong adhesive contacts in high pH solutions (pH = 12) [100]. The measurements in this thesis were performed with rough, polycrystalline calcite surfaces. Due to a large interest in interactions between calcite surfaces, spanning from geology to materials science, the potential future work should also involve preparation of smoother calcite surfaces suitable for the SFA measurements, in order to eliminate the effect of roughness on both surface forces and calcite reactivity. It is especially crucial to identify if the observed precipitation fronts in confined regions can develop in a similar fashion between smoother or single crystal calcite surfaces. Lastly, potential future work should focus on studying interactions between calcite surfaces in salt solutions with other geologically-relevant ionic composition (such as SO_4^{2-}), and in solutions containing other soluble organic molecules. According to our measurements, the organic molecules seem to be promising in switching surface forces between calcite surfaces from repulsive to attractive in weakly basic solutions.

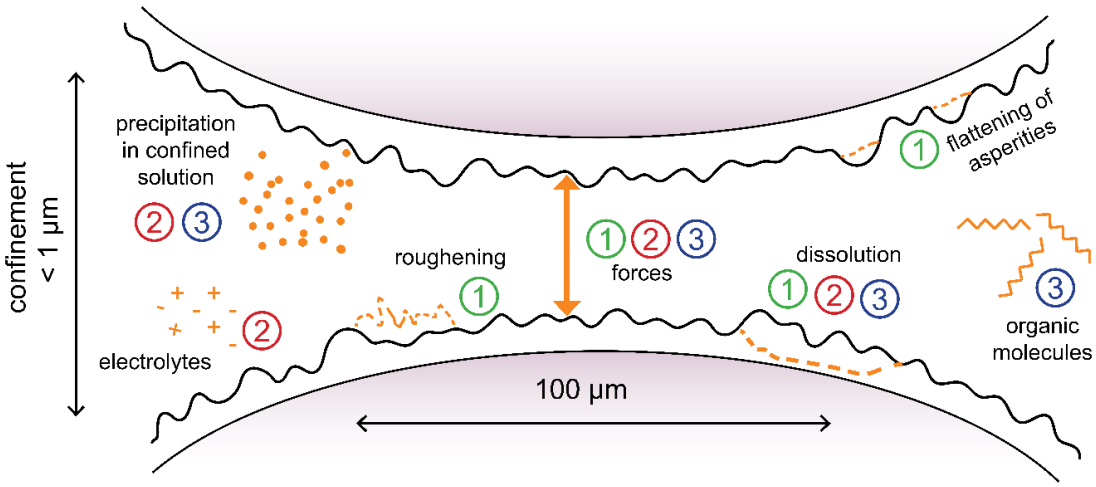

Figure 12. *Overview of the main processes studied in the SFA experiments with rough and reactive calcite surfaces in Manuscripts 1, 2 and 3. The diameter of the nominal contact area is ~100 µm and the maximum separation between the surfaces during the force-distance measurements is usually < 1 µm on retraction.*

REFERENCES

1. Kawano, J., et al., *Precipitation diagram of calcium carbonate polymorphs: its construction and significance*. Journal of Physics: Condensed Matter, 2009. **21**(42): p. 425102.
2. Wilson, J.L., *Carbonate facies in geologic history*. 2012: Springer Science & Business Media.
3. Appelo, C.A.J. and D. Postma, *Geochemistry, groundwater and pollution*. 2004: CRC press.
4. Croize, D., F. Renard, and J.-P. Gratier, *Compaction and porosity reduction in carbonates: A review of observations, theory, and experiments*. Advances in Geophysics, 2013. **54**: p. 181-238.
5. Harris, P.M., C.G.S.C. Kendall, and I. Lerche, *Carbonate cementation—a brief review*. 1985.
6. Zalasiewicz, J., *Rocks: A Very Short Introduction*. 2016: Oxford University Press.
7. Parkhurst, D.L. and C. Appelo, *Description of input and examples for PHREEQC version 3: a computer program for speciation, batch-reaction, one-dimensional transport, and inverse geochemical calculations*. 2013, US Geological Survey.
8. Brantut, N., et al., *Mechanisms of time-dependent deformation in porous limestone*. Journal of Geophysical Research: Solid Earth, 2014. **119**(7): p. 5444-5463.
9. Vajdova, V., P. Baud, and T.f. Wong, *Compaction, dilatancy, and failure in porous carbonate rocks*. Journal of Geophysical Research: Solid Earth, 2004. **109**(B5).
10. Bjørlykke, K., M. Ramm, and G.C. Saigal, *Sandstone diagenesis and porosity modification during basin evolution*. Geologische Rundschau, 1989. **78**(1): p. 243-268.
11. Scholle, P.A. and R.B. Halley, *Burial diagenesis: out of sight, out of mind!* The Society of Economic Paleolontologists and Mineralogists, Carbonate Cements, 1985. **SP36**.
12. Croizé, D., et al., *Petrophysical properties of bioclastic platform carbonates: implications for porosity controls during burial*. Marine and Petroleum Geology, 2010. **27**(8): p. 1765-1774.
13. Fruth, L., G. Orme, and F. Donath, *Experimental compaction effects in carbonate sediments*. Journal of Sedimentary Research, 1966. **36**(3): p. 747-754.
14. Ebhardt, G., *Experimental compaction of carbonate sediments*, in *Recent Developments in Carbonate Sedimentology in Central Europe*. 1968, Springer. p. 58-65.
15. Chuhan, F.A., et al., *Experimental compression of loose sands: relevance to porosity reduction during burial in sedimentary basins*. Canadian Geotechnical Journal, 2003. **40**(5): p. 995-1011.
16. Zhang, X. and C. Spiers, *Compaction of granular calcite by pressure solution at room temperature and effects of pore fluid chemistry*. International Journal of Rock Mechanics and Mining Sciences, 2005. **42**(7-8): p. 950-960.
17. Baker, P., et al., *Pressure solution and hydrothermal recrystallization of carbonate sediments—an experimental study*. Marine Geology, 1980. **38**(1-3): p. 185-203.
18. Hellmann, R., et al., *Experimental pressure solution compaction of chalk in aqueous solutions. Part 1. Deformation behavior and chemistry*. Water-rock interactions, ore deposits, and environmental geochemistry: A tribute to David A. Crerar, 2002. **7**: p. 129-152.
19. Nicolas, A., et al., *Brittle and semi-brittle behaviours of a carbonate rock: influence of water and temperature*. Geophysical Journal International, 2016. **206**(1): p. 438-456.

20. Andrew, M., B. Bijeljic, and M.J. Blunt, *Pore-scale imaging of geological carbon dioxide storage under in situ conditions*. Geophysical Research Letters, 2013. **40**(15): p. 3915-3918.
21. Budd, D.A., *The relative roles of compaction and early cementation in the destruction of permeability in carbonate grainstones: a case study from the Paleogene of west-central Florida, USA*. Journal of Sedimentary Research, 2002. **72**(1): p. 116-128.
22. Nagel, N., *Compaction and subsidence issues within the petroleum industry: From Wilmington to Ekofisk and beyond*. Physics and Chemistry of the Earth, Part A: Solid Earth and Geodesy, 2001. **26**(1-2): p. 3-14.
23. Tesei, T., et al., *Fault architecture and deformation mechanisms in exhumed analogues of seismogenic carbonate-bearing thrusts*. Journal of Structural Geology, 2013. **55**: p. 167-181.
24. Renard, F., J.-P. Gratier, and B. Jamtveit, *Kinetics of crack-sealing, intergranular pressure solution, and compaction around active faults*. Journal of Structural Geology, 2000. **22**(10): p. 1395-1407.
25. Diao, Y. and R.M. Espinosa-Marzal, *The role of water in fault lubrication*. Nature Communications, 2018. **9**(1): p. 2309.
26. Chen, J. and C.J. Spiers, *Rate and state frictional and healing behavior of carbonate fault gouge explained using microphysical model*. Journal of Geophysical Research: Solid Earth, 2016. **121**(12): p. 8642-8665.
27. Siman-Tov, S., et al., *Nanograins form carbonate fault mirrors*. Geology, 2013. **41**(6): p. 703-706.
28. Maugis, D., *Subcritical crack growth, surface energy, fracture toughness, stick-slip and embrittlement*. Journal of Materials Science, 1985. **20**(9): p. 3041-3073.
29. Røyne, A., J. Bisschop, and D.K. Dysthe, *Experimental investigation of surface energy and subcritical crack growth in calcite*. Journal of Geophysical Research: Solid Earth, 2011. **116**(B4).
30. Gratier, J.-P., F. Renard, and P. Labaume, *How pressure solution creep and fracturing processes interact in the upper crust to make it behave in both a brittle and viscous manner*. Journal of Structural Geology, 1999. **21**(8-9): p. 1189-1197.
31. Zhang, X., C.J. Spiers, and C.J. Peach, *Compaction creep of wet granular calcite by pressure solution at 28 C to 150 C*. Journal of Geophysical Research: Solid Earth, 2010. **115**(B9).
32. Angheluta, L., J. Mathiesen, and E. Aharonov, *Compaction of porous rock by dissolution on discrete stylolites: A one-dimensional model*. Journal of Geophysical Research: Solid Earth, 2012. **117**(B8).
33. Weyl, P.K., *Pressure solution and the force of crystallization: a phenomenological theory*. Journal of Geophysical Research, 1959. **64**(11): p. 2001-2025.
34. Rutter, E. and D. Elliott, *The kinetics of rock deformation by pressure solution*. Philosophical Transactions for the Royal Society of London. Series A, Mathematical and Physical Sciences, 1976: p. 203-219.
35. Gundersen, E., et al., *Coupling between pressure solution creep and diffusive mass transport in porous rocks*. Journal of Geophysical Research: Solid Earth, 2002. **107**(B11).
36. Rolland, A., et al., *Morphological analysis of stylolites for paleostress estimation in limestones*. International Journal of Rock Mechanics and Mining Sciences, 2014. **67**: p. 212-225.
37. Toussaint, R., et al., *Stylolites: A review*. Journal of Structural Geology, 2018.
38. Lehner, F. and J. Bataille, *Nonequilibrium thermodynamics of pressure solution*. Pure and Applied Geophysics, 1984. **122**(1): p. 53-85.

39. Renard, F. and P. Ortoleva, *Water films at grain-grain contacts: Debye-Hückel, osmotic model of stress, salinity, and mineralogy dependence*. Geochimica et Cosmochimica Acta, 1997. **61**(10): p. 1963-1970.
40. Butt, H.-J. and M. Kappl, *Surface and interfacial forces*. 2018: John Wiley & Sons.
41. Diao, Y. and R.M. Espinosa-Marzal, *Molecular insight into the nanoconfined calcite–solution interface*. Proceedings of the National Academy of Sciences, 2016. **113**(43): p. 12047-12052.
42. Pashley, R.M., *Hydration forces between mica surfaces in aqueous-electrolyte solutions*. Journal of Colloid and Interface Science, 1981. **80**(1): p. 153-162.
43. Pashley, R. and J. Israelachvili, *DLVO and hydration forces between mica surfaces in Mg^{2+}, Ca^{2+}, Sr^{2+}, and Ba^{2+} chloride solutions*. Journal of Colloid and Interface Science, 1984. **97**(2): p. 446-455.
44. Røyne, A., K.N. Dalby, and T. Hassenkam, *Repulsive hydration forces between calcite surfaces and their effect on the brittle strength of calcite-bearing rocks*. Geophysical Research Letters, 2015. **42**(12): p. 4786-4794.
45. Israelachvili, J.N., *Intermolecular and surface forces*. 2015: Academic press.
46. Renard, F., P. Ortoleva, and J.P. Gratier, *Pressure solution in sandstones: influence of clays and dependence on temperature and stress*. Tectonophysics, 1997. **280**(3-4): p. 257-266.
47. Alcantar, N., J. Israelachvili, and J. Boles, *Forces and ionic transport between mica surfaces: Implications for pressure solution*. Geochimica et Cosmochimica Acta, 2003. **67**(7): p. 1289-1304.
48. Heidug, W.K., *Intergranular solid-fluid phase transformations under stress: The effect of surface forces*. Journal of Geophysical Research: Solid Earth, 1995. **100**(B4): p. 5931-5940.
49. Berg, H.C., *Random walks in biology*. 1993: Princeton University Press.
50. Renard, F., et al., *An integrated model for transitional pressure solution in sandstones*. Tectonophysics, 1999. **312**(2-4): p. 97-115.
51. Dysthe, D., et al., *Fluid in mineral interfaces—molecular simulations of structure and diffusion*. Geophysical Research Letters, 2002. **29**(7).
52. van Noort, R., H.J. Visser, and C.J. Spiers, *Influence of grain boundary structure on dissolution controlled pressure solution and retarding effects of grain boundary healing*. Journal of Geophysical Research: Solid Earth, 2008. **113**(B3).
53. Van Noort, R., C. Spiers, and C. Peach, *Effects of orientation on the diffusive properties of fluid-filled grain boundaries during pressure solution*. Physics and Chemistry of Minerals, 2007. **34**(2): p. 95-112.
54. Zubtsov, S., et al., *Single-contact pressure solution creep on calcite monocrystals*. Geological Society, London, Special Publications, 2005. **243**(1): p. 81-95.
55. Stephens, C.J., et al., *Amorphous calcium carbonate is stabilized in confinement*. Advanced Functional Materials, 2010. **20**(13): p. 2108-2115.
56. Ben-Itzhak, L.L., J. Erez, and E. Aharonov, *Precipitation of $CaCO_3$ in pressure solution experiments: The importance of damage and stress*. Earth and Planetary Science Letters, 2016. **434**: p. 30-41.
57. Risnes, R., et al., *Water weakening of chalk—Mechanical effects of water–glycol mixtures*. Journal of Petroleum Science and Engineering, 2005. **48**(1): p. 21-36.
58. Nermoen, A., et al., *Porosity and permeability development in compacting chalks during flooding of nonequilibrium brines: Insights from long-term experiment*. Journal of Geophysical Research: Solid Earth, 2015. **120**(5): p. 2935-2960.
59. Burshtein, L., *Effect of moisture on the strength and deformability of sandstone*. Journal of Mining Science, 1969. **5**(5): p. 573-576.

60. Waza, T., K. Kurita, and H. Mizutani, *The effect of water on the subcritical crack growth in silicate rocks*. Tectonophysics, 1980. **67**(1-2): p. 25-34.
61. Rutter, E.H., *The influence of interstitial water on the rheological behaviour of calcite rocks*. Tectonophysics, 1972. **14**(1): p. 13-33.
62. Orowan, E., *The fatigue of glass under stress*. Nature, 1944. **154**(3906): p. 341-343.
63. Michalske, T.A. and S.W. Freiman, *A molecular interpretation of stress corrosion in silica*. Nature, 1982. **295**(5849): p. 511-512.
64. Wong, L. and V. Maruvanchery, *Water effects on rocks*. Rock Mechanics and Rock Engineering: From the Past to the Future, 2016: p. 187.
65. Newman, G.H., *The effect of water chemistry on the laboratory compression and permeability characteristics of some North Sea chalks*. Journal of Petroleum Technology, 1983. **35**(05): p. 976-980.
66. Delage, P., C. Schroeder, and Y.J. Cui, *Subsidence and capillary effects in chalks*. arXiv preprint arXiv:0803.1308, 2008.
67. Nermoen, A., et al., *Incorporating electrostatic effects into the effective stress relation—Insights from chalk experiments*. Geophysics, 2018. **83**(3): p. MR123-MR135.
68. Megawati, M., A. Hiorth, and M.V. Madland, *The impact of surface charge on the mechanical behavior of high-porosity chalk*. Rock Mechanics and Rock Engineering, 2013. **46**: p. 1073-1090.
69. Hiorth, A., L. Cathles, and M. Madland, *The impact of pore water chemistry on carbonate surface charge and oil wettability*. Transport in Porous Media, 2010. **85**(1): p. 1-21.
70. Risnes, R. and O. Flaageng, *Mechanical properties of chalk with emphasis on chalk-fluid interactions and micromechanical aspects*. Oil & Gas Science and Technology, 1999. **54**(6): p. 751-758.
71. Risnes, R., et al., *Chalk–fluid interactions with glycol and brines*. Tectonophysics, 2003. **370**(1-4): p. 213-226.
72. Madland, M., et al., *Chemical alterations induced by rock–fluid interactions when injecting brines in high porosity chalks*. Transport in Porous Media, 2011. **87**(3): p. 679-702.
73. Lakshtanov, L., et al., *Limits on calcite and chalk recrystallization*. Crystal Growth & Design, 2018. **18**(8): p. 4536-4543.
74. Hassenkam, T., L.L. Skovbjerg, and S.L.S. Stipp, *Probing the intrinsically oil-wet surfaces of pores in North Sea chalk at subpore resolution*. Proceedings of the National Academy of Sciences, 2009. **106**(15): p. 6071-6076.
75. Matthiesen, J., et al., *Adsorbed organic material and its control on wettability*. Energy & Fuels, 2016. **31**(1): p. 55-64.
76. Pedersen, N., et al., *Low salinity effect at pore scale: Probing wettability changes in Middle East Limestone*. Energy & Fuels, 2016. **30**(5): p. 3768-3775.
77. Matthiesen, J., et al., *How naturally adsorbed material on minerals affects low salinity enhanced oil recovery*. Energy & Fuels, 2014. **28**(8): p. 4849-4858.
78. Austad, T., et al., *Conditions for a low-salinity enhanced oil recovery (EOR) effect in carbonate oil reservoirs*. Energy & Fuels, 2011. **26**(1): p. 569-575.
79. Alroudhan, A., J. Vinogradov, and M. Jackson, *Zeta potential of intact natural limestone: Impact of potential-determining ions Ca, Mg and SO_4*. Colloids and Surfaces A: Physicochemical and Engineering Aspects, 2016. **493**: p. 83-98.
80. Fathi, S.J., T. Austad, and S. Strand, *"Smart water" as a wettability modifier in chalk: the effect of salinity and ionic composition*. Energy & fuels, 2010. **24**(4): p. 2514-2519.
81. Gomari, K.R. and A. Hamouda, *Effect of fatty acids, water composition and pH on the wettability alteration of calcite surface*. Journal of Petroleum Science and Engineering, 2006. **50**(2): p. 140-150.

82. Buckley, J.S., *Effective wettability of minerals exposed to crude oil*. Current Opinion in Colloid & Interface Science, 2001. **6**(3): p. 191-196.
83. Eichmann, S.L. and N.A. Burnham, *Calcium-mediated adhesion of nanomaterials in reservoir fluids*. Scientific Reports, 2017. **7**(1): p. 11613.
84. Rios-Carvajal, T., et al., *Specific ion effects on the interaction of hydrophobic and hydrophilic self-assembled monolayers*. Langmuir, 2018. **34**(35): p. 10254-10261.
85. Deraguin, B. and L. Landau, *Theory of the stability of strongly charged lyophobic sols and of the adhesion of strongly charged particles in solution of electrolytes*. Acta Physicochim: USSR, 1941. **14**: p. 633-662.
86. Verwey, J. and T. Overbeek, *Theory of the stability of lyophobic colloids*. Advances in Colloid Interface Science. Elsevier: Amsterdam, 1948. **17**.
87. Lifshitz, E., *The theory of molecular attractive forces between solids*. 1956.
88. Bergström, L., *Hamaker constants of inorganic materials*. Advances in Colloid and Interface Science, 1997. **70**: p. 125-169.
89. Bergaya, F. and G. Lagaly, *Handbook of clay science*. Vol. 5. 2013: Newnes.
90. Trefalt, G., F.J.M. Ruiz-Cabello, and M. Borkovec, *Interaction forces, heteroaggregation, and deposition involving charged colloidal particles*. The Journal of Physical Chemistry B, 2014. **118**(23): p. 6346-6355.
91. Parsons, D.F. and B.W. Ninham, *Charge reversal of surfaces in divalent electrolytes: The role of ionic dispersion interactions*. Langmuir, 2010. **26**(9): p. 6430-6436.
92. Donaldson Jr, S.H., et al., *Developing a general interaction potential for hydrophobic and hydrophilic interactions*. Langmuir, 2014. **31**(7): p. 2051-2064.
93. Javadi, S. and A. Røyne, *Adhesive forces between two cleaved calcite surfaces in NaCl solutions: the importance of ionic strength and normal loading*. Journal of Colloid and Interface Science, 2018.
94. Heuberger, M., et al., *Collective dehydration of ions in nano-pores*. Physical Chemistry Chemical Physics, 2017. **19**(21): p. 13462-13468.
95. Grabbe, A. and R.G. Horn, *Double-layer and hydration forces measured between silica sheets subjected to various surface treatments*. Journal of Colloid and Interface Science, 1993. **157**(2): p. 375-383.
96. Parsegian, V. and T. Zemb, *Hydration forces: Observations, explanations, expectations, questions*. Current Opinion in Colloid & Interface Science, 2011. **16**(6): p. 618-624.
97. Wennerström, H., B. Jönsson, and P. Linse, *The cell model for polyelectrolyte systems. Exact statistical mechanical relations, Monte Carlo simulations, and the Poisson–Boltzmann approximation*. The Journal of Chemical Physics, 1982. **76**(9): p. 4665-4670.
98. Kjellander, R., et al., *Double-layer ion correlation forces restrict calcium-clay swelling*. The Journal of Physical Chemistry, 1988. **92**(23): p. 6489-6492.
99. Oosawa, F., *Polyelectrolytes*, in *Polyelectrolytes*. 1971, Marcel Dekker.
100. Pourchet, S., et al., *Chemistry of the calcite/water interface: influence of sulfate ions and consequences in terms of cohesion forces*. Cement and Concrete Research, 2013. **52**: p. 22-30.
101. Wolthers, M., L. Charlet, and P. Van Cappellen, *The surface chemistry of divalent metal carbonate minerals; a critical assessment of surface charge and potential data using the charge distribution multi-site ion complexation model*. American Journal of Science, 2008. **308**(8): p. 905-941.
102. Lee, S.S., et al., *Surface charge of the calcite (104) terrace measured by Rb^+ adsorption in aqueous solutions using resonant anomalous X-ray reflectivity*. The Journal of Physical Chemistry C, 2016. **120**(28): p. 15216-15223.
103. Stipp, S., *Toward a conceptual model of the calcite surface: hydration, hydrolysis, and surface potential*. Geochimica et Cosmochimica Acta, 1999. **63**(19): p. 3121-3131.

104. Stipp, S.L. and M.F. Hochella, *Structure and bonding environments at the calcite surface as observed with X-ray photoelectron spectroscopy (XPS) and low energy electron diffraction (LEED)*. Geochimica et Cosmochimica Acta, 1991. **55**(6): p. 1723-1736.
105. Bohr, J., et al., *Thickness and structure of the water film deposited from vapour on calcite surfaces*. Geochimica et Cosmochimica Acta, 2010. **74**(21): p. 5985-5999.
106. Geissbühler, P., et al., *Three-dimensional structure of the calcite–water interface by surface X-ray scattering*. Surface Science, 2004. **573**(2): p. 191-203.
107. Brekke-Svaland, G. and F. Bresme, *Interactions between hydrated calcium carbonate surfaces at nanoconfinement conditions*. The Journal of Physical Chemistry C, 2018.
108. Parsons, D.F., R.B. Walsh, and V.S. Craig, *Surface forces: Surface roughness in theory and experiment*. The Journal of Chemical Physics, 2014. **140**(16): p. 164701.
109. Eom, N., D.F. Parsons, and V.S. Craig, *Roughness in surface force measurements: Extension of DLVO theory to describe the forces between hafnia surfaces*. The Journal of Physical Chemistry B, 2017.
110. Røyne, A. and D.K. Dysthe, *Rim formation on crystal faces growing in confinement*. Journal of Crystal Growth, 2012. **346**(1): p. 89-100.
111. Li, L., et al., *Growth of calcite in confinement*. Crystals, 2017. **7**(12): p. 361.
112. Putnis, A., *Transient porosity resulting from fluid–mineral interaction and its consequences*. Reviews in Mineralogy and Geochemistry, 2015. **80**(1): p. 1-23.
113. Prieto, M., *Nucleation and supersaturation in porous media (revisited)*. Mineralogical Magazine, 2014. **78**(6): p. 1437-1448.
114. Hedges, L.O. and S. Whitelam, *Patterning a surface so as to speed nucleation from solution*. Soft Matter, 2012. **8**(33): p. 8624-8635.
115. Zeng, M., et al., *Confinement generates single-crystal aragonite rods at room temperature*. Proceedings of the National Academy of Sciences, 2018: p. 201718926.
116. Tegethoff, F.W., J. Rohleder, and E. Kroker, *Calcium carbonate: from the Cretaceous period into the 21st century*. 2001: Springer Science & Business Media.
117. da Fonseca, B.S., et al., *Development of formulations based on TEOS-dicarboxylic acids for consolidation of carbonate stones*. New Journal of Chemistry, 2016. **40**(9): p. 7493-7503.
118. Wu, B., et al., *Effect of Ca^{2+} ion concentration on adsorption of poly (carboxylate ether)-based (PCE) superplasticizer on mica*. Journal of Colloid and Interface Science, 2018. **527**: p. 195-201.
119. Karlkvist, T., et al., *Flotation selectivity of novel alkyl dicarboxylate reagents for apatite–calcite separation*. Journal of Colloid and Interface Science, 2015. **445**: p. 40-47.
120. Piekarska, K., E. Piorkowska, and J. Bojda, *The influence of matrix crystallinity, filler grain size and modification on properties of PLA/calcium carbonate composites*. Polymer Testing, 2017. **62**: p. 203-209.
121. Jiang, L., J. Zhang, and M.P. Wolcott, *Comparison of polylactide/nano-sized calcium carbonate and polylactide/montmorillonite composites: reinforcing effects and toughening mechanisms*. Polymer, 2007. **48**(26): p. 7632-7644.
122. Srivabut, C., T. Ratanawilai, and S. Hiziroglu, *Effect of nanoclay, talcum, and calcium carbonate as filler on properties of composites manufactured from recycled polypropylene and rubberwood fiber*. Construction and Building Materials, 2018. **162**: p. 450-458.
123. Sepulcre-Guilabert, J., T.P. Ferrándiz-Gómez, and J.M. Martín-Martínez, *Properties of polyurethane adhesives containing natural calcium carbonate +fumed silica mixtures*. Journal of Adhesion Science and Technology, 2001. **15**(2): p. 187-203.
124. Gao, X., et al., *Synthesis and characterization of well-dispersed polyurethane/$CaCO_3$ nanocomposites*. Colloids and Surfaces A: Physicochemical and Engineering Aspects, 2010. **371**(1-3): p. 1-7.

125. Donate-Robles, J. and J.M. Martín-Martínez, *Addition of precipitated calcium carbonate filler to thermoplastic polyurethane adhesives*. International Journal of Adhesion and Adhesives, 2011. **31**(8): p. 795-804.
126. Tabtiang, A. and R. Venables, *The performance of selected unsaturated coatings for calcium carbonate filler in polypropylene*. European Polymer Journal, 2000. **36**(1): p. 137-148.
127. Alvarez, V. and M. Paulis, *Effect of acrylic binder type and calcium carbonate filler amount on the properties of paint-like blends*. Progress in Organic Coatings, 2017. **112**: p. 210-218.
128. Rogan, K., et al., *Colloidal stability of calcite dispersion treated with sodium polyacrylate*. Colloid and Polymer Science, 1994. **272**(10): p. 1175-1189.
129. Nehdi, M., *Why some carbonate fillers cause rapid increases of viscosity in dispersed cement-based materials*. Cement and concrete Research, 2000. **30**(10): p. 1663-1669.
130. Neto, C.S. and V.C. Campiteli, *The influence of limestone additions on the rheological properties and water retention value of Portland cement slurries*, in *Carbonate additions to cement*. 1990, ASTM International.
131. Nehdi, M., S. Mindess, and P.-C. Aıtcin, *Rheology of high-performance concrete: effect of ultrafine particles*. Cement and Concrete Research, 1998. **28**(5): p. 687-697.
132. Finnemore, A., et al., *Biomimetic layer-by-layer assembly of artificial nacre*. Nature Communications, 2012. **3**: p. 966.
133. Nudelman, F. and N.A. Sommerdijk, *Biomineralization as an inspiration for materials chemistry*. Angewandte Chemie International Edition, 2012. **51**(27): p. 6582-6596.
134. Geffroy, C., et al., *Surface complexation of calcite by carboxylates in water*. Journal of Colloid and Interface Science, 1999. **211**(1): p. 45-53.
135. Compton, R.G. and C.A. Brown, *The inhibition of calcite dissolution/precipitation: 1, 2-dicarboxylic acids*. Journal of Colloid and Interface Science, 1995. **170**(2): p. 586-590.
136. Reddy, M.M. and A.R. Hoch, *Calcite crystal growth rate inhibition by polycarboxylic acids*. Journal of Colloid and Interface Science, 2001. **235**(2): p. 365-370.
137. Salinas-Nolasco, M.F., et al., *Passivation of the calcite surface with malonate ion*. Journal of Colloid and Interface Science, 2004. **274**(1): p. 16-24.
138. Teng, H.H., Y. Chen, and E. Pauli, *Direction specific interactions of 1, 4-dicarboxylic acid with calcite surfaces*. Journal of the American Chemical Society, 2006. **128**(45): p. 14482-14484.
139. Thomas, M.M., J.A. Clouse, and J.M. Longo, *Adsorption of organic compounds on carbonate minerals: 1. Model compounds and their influence on mineral wettability*. Chemical Geology, 1993. **109**(1-4): p. 201-213.
140. Wada, N., K. Kanamura, and T. Umegaki, *Effects of carboxylic acids on the crystallization of calcium carbonate*. Journal of Colloid and Interface Science, 2001. **233**(1): p. 65-72.
141. Hakim, S., et al., *Interactions of the calcite {10.4} surface with organic compounds: structure and behaviour at mineral–organic interfaces*. Scientific Reports, 2017. **7**(1): p. 7592.
142. Ataman, E., et al., *Functional group adsorption on calcite: I. Oxygen containing and nonpolar organic molecules*. The Journal of Physical Chemistry C, 2016. **120**(30): p. 16586-16596.
143. Ataman, E., et al., *Functional group adsorption on calcite: II. Nitrogen and sulfur containing organic molecules*. The Journal of Physical Chemistry C, 2016. **120**(30): p. 16597-16607.
144. Freeman, C.L., et al., *Interactions of organic molecules with calcite and magnesite surfaces*. The Journal of Physical Chemistry C, 2009. **113**(9): p. 3666-3673.
145. Stipp, S.L.S., *Toward a conceptual model of the calcite surface: hydration, hydrolysis, and surface potential*. Geochimica et Cosmochimica Acta, 1999. **63**(19-20): p. 3121-3131.

146. Bovet, N., et al., *Interaction of alcohols with the calcite surface.* Physical Chemistry Chemical Physics, 2015. **17**(5): p. 3490-3496.
147. Chaussemier, M., et al., *State of art of natural inhibitors of calcium carbonate scaling. A review article.* Desalination, 2015. **356**: p. 47-55.
148. Israelachvili, J., et al., *Recent advances in the surface forces apparatus (SFA) technique.* Reports on Progress in Physics, 2010. **73**(3).
149. Israelachvili, J.N. and D. Tabor, *The measurement of van der Waals dispersion forces in the range 1.5 to 130 nm.* Proc. R. Soc. Lond. A, 1972. **331**(1584): p. 19-38.
150. Israelachvili, J.N. and G.E. Adams, *Measurement of Forces between 2 Mica Surfaces in Aqueous-Electrolyte Solutions in Range 0-100 Nm.* Journal of the Chemical Society-Faraday Transactions I, 1978. **74**: p. 975-&.
151. Heuberger, M., G. Luengo, and J. Israelachvili, *Topographic information from multiple beam interferometry in the surface forces apparatus.* Langmuir, 1997. **13**(14): p. 3839-3848.
152. Tadmor, R., N. Chen, and J.N. Israelachvili, *Thickness and refractive index measurements using multiple beam interference fringes (FECO).* Journal of Colloid and Interface Science, 2003. **264**(2): p. 548-553.
153. Tolansky, S., *Multiple-beam interferometry of surfaces and films*. 1970: Dover Publications.
154. Israelachvili, J.N., *Thin film studies using multiple-beam interferometry.* Journal of Colloid and Interface Science, 1973. **44**(2): p. 259-272.
155. Horn, R., D. Smith, and W. Haller, *Surface forces and viscosity of water measured between silica sheets.* Chemical Physics Letters, 1989. **162**(4-5): p. 404-408.
156. Teng, F., H. Zeng, and Q. Liu, *Understanding the deposition and surface interactions of gypsum.* The Journal of Physical Chemistry C, 2011. **115**(35): p. 17485-17494.
157. Horn, R., D. Clarke, and M. Clarkson, *Direct measurement of surface forces between sapphire crystals in aqueous solutions.* Journal of Materials Research, 1988. **3**(03): p. 413-416.
158. Chen, S.-Y., et al., *Effects of salinity on oil recovery (the 'dilution effect'): Experimental and theoretical studies of crude oil/brine/carbonate surface restructuring and associated physico-chemical interactions.* Energy & Fuels, 2017.
159. Cantaert, B., et al., *Think Positive: Phase Separation Enables a Positively Charged Additive to Induce Dramatic Changes in Calcium Carbonate Morphology.* Advanced Functional Materials, 2012. **22**(5): p. 907-915.
160. Nilsen, O., F. H., and A. Kjekshus, *Growth of calcium carbonate by the atomic layer chemical vapour deposition technique.* Thin Solid Films, 2004. **450**: p. 240-247.
161. Dziadkowiec, J., et al., *Surface Forces Apparatus measurements of interactions between rough and reactive calcite surfaces.* Langmuir, 2018. **34**(25): p. 7248-7263.
162. Israelachvili, J.N., et al., *Preparing contamination-free mica substrates for surface characterization, force measurements, and imaging.* Langmuir, 2004. **20**(9): p. 3616-3622.
163. Reithmeier, M. and A. Erbe, *Dielectric interlayers for increasing the transparency of metal films for mid-infrared attenuated total reflection spectroscopy.* Physical Chemistry Chemical Physics, 2010. **12**(44): p. 14798-14803.
164. Schubert, M., *Polarization-dependent optical parameters of arbitrarily anisotropic homogeneous layered systems.* Physical Review B, 1996. **53**(8): p. 4265.
165. Hanor, J.S., *Origin of saline fluids in sedimentary basins.* Geological Society, London, Special Publications, 1994. **78**(1): p. 151-174.